July 1988 UILU-ENG-88-2235

COORDINATED SCIENCE LABORATORY
College of Engineering

ACOUSTIC PHONON SCATTERING IN MODULATION DOPED $ALUMINUM_xGALLIUM_{1-x}$ ARSENIDE/GALLIUM ARSENIDE HETEROJUNCTIONS

Stephen Joseph Manion

UNIVERSITY OF ILLINOIS AT URBANA-CHAMPAIGN

UNCLASSIFIED

SECURITY CLASSIFICATION OF THIS PAGE

REPORT DOCUMENTATION PAGE

1a. REPORT SECURITY CLASSIFICATION Unclassified	1b. RESTRICTIVE MARKINGS None
2a. SECURITY CLASSIFICATION AUTHORITY	3. DISTRIBUTION/AVAILABILITY OF REPORT Approved for public release; distribution unlimited
2b. DECLASSIFICATION/DOWNGRADING SCHEDULE	
4. PERFORMING ORGANIZATION REPORT NUMBER(S) UILU-ENG-88-2235	5. MONITORING ORGANIZATION REPORT NUMBER(S)
6a. NAME OF PERFORMING ORGANIZATION Coordinated Science Lab University of Illinois 6b. OFFICE SYMBOL (If applicable) N/A	7a. NAME OF MONITORING ORGANIZATION Office of Naval Research
6c. ADDRESS (City, State, and ZIP Code) 1101 W. Springfield Ave. Urbana, IL 61801	7b. ADDRESS (City, State, and ZIP Code) 800 N. Quincy St. Arlington, VA 22217
8a. NAME OF FUNDING/SPONSORING ORGANIZATION Joint Services Electronics Program 8b. OFFICE SYMBOL (If applicable)	9. PROCUREMENT INSTRUMENT IDENTIFICATION NUMBER N00014-84-C-0149
8c. ADDRESS (City, State, and ZIP Code) 800 N. Quincy St. Arlington, VA 22217	10. SOURCE OF FUNDING NUMBERS PROGRAM ELEMENT NO. / PROJECT NO. / TASK NO. / WORK UNIT ACCESSION NO

11. TITLE (Include Security Classification)
ACOUSTIC PHONON SCATTERING IN MODULATION DOPED ALUMINUM$_x$GALLIUM$_{1-x}$ARSENIDE/GALLIUM ARSENIDE HETEROJUNCTIONS

12. PERSONAL AUTHOR(S)
Manion, Stephen Joseph

13a. TYPE OF REPORT	13b. TIME COVERED	14. DATE OF REPORT (Year, Month, Day)	15. PAGE COUNT
Technical	FROM _____ TO _____	1988 July	100

16. SUPPLEMENTARY NOTATION

17. COSATI CODES			18. SUBJECT TERMS (Continue on reverse if necessary and identify by block number)
FIELD	GROUP	SUB-GROUP	Acoustic deformation potential scattering, Modulation doped heterojunctions, Deformation potential, Theory of scattering Power loss.

19. ABSTRACT (Continue on reverse if necessary and identify by block number)

We investigate acoustic deformation potential scattering in Al$_x$Ga$_{1-x}$As/GaAs modulation doped heterojunctions. We review previous measurements of the deformation potential constant Z and discuss the controversy over the discrepancy between the measured value of Z in bulk GaAs and in the heterojunction. By comparing the theory of scattering in bulk GaAs with previously reported measurements of the mobility at 77K we determine an upper limit for the deformation potential constant of 11 eV.

We experimentally measure the relationship between the electron temperature and the power loss, and we compare our measurements with theory. We conclude, in general agreement with previous measurements in heterojunctions, that a large value of the deformation potential constant (approximately 16 eV) would be necessary to fit the data using a theory of acoustic phonon scattering. In contrast with previously reported studies of acoustic deformation potential scattering in heterojunctions, we do not conclude that earlier measurements of Z in bulk GaAs are in error. Instead, we suggest a number of possible enhancements to the theory which may explain the anomalously large power loss which (continued on back of page)

20. DISTRIBUTION/AVAILABILITY OF ABSTRACT	21. ABSTRACT SECURITY CLASSIFICATION
☒ UNCLASSIFIED/UNLIMITED ☐ SAME AS RPT. ☐ DTIC USERS	Unclassified
22a. NAME OF RESPONSIBLE INDIVIDUAL	22b. TELEPHONE (Include Area Code) / 22c. OFFICE SYMBOL

DD FORM 1473, 84 MAR — 83 APR edition may be used until exhausted. All other editions are obsolete.

SECURITY CLASSIFICATION OF THIS PAGE

UNCLASSIFIED

19. Abstract (continued)

we observe. Our experiment, unlike previous studies of the mobility, indicates clearly that if an additional scattering mechanism is the cause, then it must be an inelastic mechanism.

We also present a comprehensive theory of the electronic power loss in the heterojunction, including the effects of screening. It is found that screening changes the temperature dependence of the power loss (or the mobility) and that this makes it possible to conclusively observe the effects of screening at low temperatures. Analytical solutions of the power loss equation are presented and the temperature range over which the analytical solution is valid is discussed. It is found that the analytical solutions are valid only at temperatures much lower than previously believed.

ACOUSTIC PHONON SCATTERING IN MODULATION DOPED $ALUMINUM_X$ $GALLIUM_{1-X}$ ARSENIDE/GALLIUM ARSENIDE HETEROJUNCTIONS

BY

STEPHEN JOSEPH MANION

B.E.E., University of Delaware, 1981
M.S., University of Illinois, 1985

THESIS

Submitted in partial fulfillment of the requirements
for the degree of Doctor of Philosophy in Electrical Engineering
in the Graduate College of the
University of Illinois at Urbana-Champaign, 1988

Urbana, Illinois

ACOUSTIC PHONON SCATTERING IN MODULATION DOPED ALUMINUM$_X$ GALLIUM$_{1-X}$ ARSENIDE/GALLIUM ARSENIDE HETEROJUNCTIONS

Stephen Joseph Manion, Ph. D.
Department of Electrical and Computer Engineering
University of Illinois at Urbana–Champaign, 1988
Professor Karl Hess, Advisor

We investigate acoustic deformation potential scattering in $Al_xGa_{1-x}As/GaAs$ modulation doped heterojunctions. We review previous measurements of the deformation potential constant Z and discuss the controversy over the discrepancy between the measured value of Z in bulk GaAs and in the heterojunction. By comparing the theory of scattering in bulk GaAs with previously reported measurements of the mobility at 77 K we determine an upper limit for the deformation potential constant of 11 eV.

We experimentally measure the relationship between the electron temperature and the power loss, and we compare our measurements with theory. We conclude, in general agreement with previous measurements in heterojunctions, that a large value of the deformation potential constant (approximately 16 eV) would be necessary to fit the data using a theory of acoustic phonon scattering. In contrast with previously reported studies of acoustic deformation potential scattering in heterojunctions, we do not conclude that earlier measurements of Z in bulk GaAs are in error. Instead, we suggest a number of possible enhancements to the theory which may explain the anomalously large power loss which we observe. Our experiment, unlike previous studies of the mobility, indicates clearly that if an additional scattering mechanism is the cause, then it must be an inelastic mechanism.

We also present a comprehensive theory of the electronic power loss in the heterojunction, including the effects of screening. It is found that screening changes the temperature dependence of the power loss (or the mobility) and that this makes it possible to conclusively observe the effects of screening at low temperatures. Analytical solutions of the power loss equation are presented and the temperature range over which the analytical solution is valid is discussed. It is found that the analytical solutions are valid only at temperatures much lower then previously believed.

ACKNOWLEDGMENTS

I would like first to thank my advisor, Professor Karl Hess, for his guidance and support during this research. I have found his insistence on precision in writing and speaking to be an invaluable aid to the clarification of my ideas; his philosophy of research will be of assistance to me no matter what problem I am working on.

I would also like to thank Professor James Coleman, who has helped in many ways. His group grew the crystals which I have used in my research, and he has provided valuable insights into this and other work. He also generously provided the financial support for me to attend the Device Research Conference during 1987.

Thanks are due to Professor Gregory Stillman, for his help in understanding acoustic phonon scattering in bulk GaAs and his assistance in contacting potential employers, and to Professor Joseph Lyding, for his stimulating conversations and his contributions to our vain attempt to win an intramural basketball championship. The time and input of all the members of my committee have been greatly appreciated.

I am indebted to Professor Jean–Pierre Leburton and Dr. Bruce Mason for taking the time to read papers of mine before I submitted them for publication. My prose was considerably more graceful because of their efforts. I would like to acknowledge the assistance of Dr. Mark Emanuael and Dr. Gregory Costrini, who grew most of the crystals used in my research, and without whom this research would not have been possible. Dr. Mike Artaki, Dan Bailey, and Işik Kizilyalli have all offered considerable help on various aspects of semiconductor theory. Dr. Michael Haase, Dr. Virginia Robbins, Ted Higman, and Mike Favaro have provided friendship and support as well as the odd piece of

equipment or advice necessary to make my experiments work. I have had considerably more fun at the University because of the friendship of many people. Of special note are Linda Miller, John Scott, D.D.S., The Dead Fish (Jerome Hubacek, Matt Kim, Lou Guido, Tom Rudnick, Brian Cunningham, and others already mentioned) as well as Jack Higman, Mike Givens, Pam York, Jim Baillargeon, Gloria Fernandez, Caroline Larsen, Alice Wuellner, Rob Bryan, Steve Briggs, Doug Arnold, Dr. Chris Stanton, Ki Wook Kim Sylvia and Ken Patterson, Kevin Beernink, Al Hanson, Chuck Zmudzinski, Tony Tang, Greg Lyons, and Dennis Deppe.

Mrs. E. Kesler has always found me to inform me of group activities, even when I was far from my office, and has always cheerfully typed anything I needed. Her help was greatly appreciated.

My parents deserve a special thanks for instilling in me the curiosity which led to my pursuit of an advanced degree. Other members of my family, especially Terry, Jeff, Deirdre, and Charlie have also offered both support and encouragement, which has been greatly appreciated.

This work was supported by the Joint Services Electronic Program and the Office of Naval Research.

Table of Contents

1. INTRODUCTION

Heterostructures and electron transport within them have been of interest for as long as semiconductors have been studied. In 1951, shortly after the invention of the transistor, Shockley patented a transistor design that used a heterojunction band discontinuity at the emitter–base junction to improve the efficiency of the charge injection.[1] But the crystal growth technologies in use at the time were inadequate for the growth of this device, or of any other heterostructure device. As a result, the development of heterojunction devices was not actively pursued.

Over the past fifteen years the growth technologies have improved considerably. Metal Organic Chemical Vapor Deposition (MOCVD)[2] and Molecular Beam Epitaxy (MBE)[3] have matured into reliable techniques for the growth of high quality heterostructures. A number of companies manufacture standardized systems which can be used to grow structures with abrupt interfaces, precisely controlled thicknesses and doping levels, and a minimal number of interface defects. This has led to a resurgence of interest in heterojunctions. The development of MOCVD is particularly important, as it allows commercial users to produce heterostructures in large volume and at reasonable cost.

The design of heterostructure devices such as High Electron Mobility Transistors (HEMTs)[4] or real space transfer devices[5] requires a detailed understanding of the mechanisms that govern transport. Experimental measurements of the transport properties are therefore of primary importance. In this thesis we focus on measuring the effects of acoustic deformation potential scattering, an important mechanism at low temperatures in modulation doped heterojunctions. Although the basic scattering mechanism is

the same as in bulk material, experimental measurements of the strength of the scattering in bulk GaAs and in modulation doped $Al_xGa_{1-x}As$/GaAs structures disagree considerably, suggesting that acoustic phonon scattering in heterojunctions is not fully understood.

Our study reveals something of the physical mechanism behind the discrepancies between recent measurements of the acoustic deformation potential constant Z in modulation doped $Al_xGa_{1-x}As$/GaAs heterostructures and the measurement of Z in bulk GaAs. Modulation doped heterostructures are used both to implement the HEMT and to investigate such novel physical effects as the quantum Hall effect,[6] and are therefore of considerable interest. The acoustic deformation potential constant determines the strength of the interaction between the electrons and the acoustic phonons. Whereas in previous studies the value of Z has been inferred from measurements of the mobility, we determine Z by comparing our measurements of the rate at which the conduction electrons lose excess energy with theoretical calculations. Our measurements are more reliably interpreted because the power loss is unaffected by the elastic scattering mechanisms which complicate the analysis of mobility measurements.

In the next chapter we review previous measurements of Z, both in bulk GaAs and in $Al_xGa_{1-x}As$/GaAs heterojunctions, and we introduce the method of measuring Z from the power loss of electrons. We then develop the theory of the power loss in a heterojunction. Excess energy is imparted by an electric field, which is assumed to change the distribution function of the electrons from a Fermi–Dirac distribution at the lattice temperature T_l to a Fermi–Dirac distribution with an elevated electron temperature T_e. The electron temperature rises until the net power loss, determined by the balance between

the power lost to phonon emission and the power gained from phonon absorption, is equal to the power input from the field. The integrals necessary to average all allowed phonon interactions over all the electrons are calculated numerically to tabulate the average power loss rate as a function of T_l and T_e. We critically evaluate some previous analytical solutions of the power loss equations, and discuss the temperature range over which the approximations necessary to an analytical solution are valid.

The experimental measurement of these quantities is discussed in chapter 4. The lattice temperature is easily measured, and, in the steady state, the average power loss per electron is the input power divided by the total number of conduction electrons. We determine the electron temperature through its strong influence on the amplitudes of the Shubnikov–de Haas oscillations.

Finally, the theoretical power loss is fit to the experimental measurements by adjusting the deformation potential constant to minimize the deviation between theory and experiment. We require a deformation potential constant of 15.8 eV to fit our data using a theory which includes screening. This is somewhat larger than the values inferred by other methods, and we discuss a number of possible explanations. A comparison of the results from mobility measurements, which are sensitive to any scattering mechanism, with our power loss measurements, which are sensitive only to inelastic scattering, provides an important clue to the possible causes of the differences between the measurements in bulk GaAs and the measurements in heterostructures.

2. ACOUSTIC PHONONS

2.1. Acoustic Phonon Scattering

An acoustic phonon traveling through a crystal deforms the crystal, and this deformation produces in III–V compounds two separate kinds of scattering potentials, the piezoelectric potential and the deformation potential. In the simplest model, each of these interactions is characterized by a single constant which relates the amount of deformation to the magnitude of the potential produced. These constants are necessary for the calculation of the acoustic phonon limited mobility, and it is important to experimentally measure them.

The piezoelectric effect describes the potential produced by the deformation of an ionic crystal which does not have a center of symmetry.[7] The deformation changes the orientation of the dipoles in each unit cell and thus produces a long range potential. For crystals having the zincblende symmetry the piezoelectric tensor has only one nonzero component.[8] The piezoelectric constant can be determined from a number of simple experiments which directly measure the deformation of a crystal and the resulting potential.[9] In GaAs, the generally accepted piezoelectric constant is believed to be accurate to two decimal places. We account for piezoelectric scattering in our work, but we will not discuss it in detail. Instead, we turn to the deformation potential constant, which cannot be measured directly, and which is not agreed on to even the first digit.

When a crystal is compressed, the change in the density of the crystal causes a change in the band gap energy which can be broken down into a shift in the conduction band edge and a shift in the valence band edge. In this work we are concerned with the

scattering of electrons by the shift of the conduction band edge. For small changes in density, the change in the conduction band energy is proportional to the compression. The deformation potential constant Z is defined by

$$\Delta E_c = Z\frac{\Delta V}{V_0} \tag{2.1}$$

where ΔE_c is the change in the conduction band energy, ΔV is the change in crystal volume, and V_0 is the equilibrium volume.[10] Longitudinal acoustic phonons, which produce periodic variations in the crystal density, can scatter electrons through the deformation potential. The scattering rate, calculated using Fermi's golden rule, is proportional to Z^2. Both the acoustic phonon limited mobility and the power loss are weighted averages of the scattering rate, and are therefore quite sensitive to the exact value of the deformation potential.

Despite the almost forty years that have passed since Bardeen and Shockley proposed the deformation potential formalism,[10] the precise value of Z in GaAs is not well known. The reported values cover an order of magnitude variation in the predicted scattering rate. The uncertainty in Z can be attributed to two things: 1) most studies have inferred a value for Z by fitting theoretical calculations of the mobility to experimental measurements, a method which suffers because of the difficulty in separating the effects of the various scattering mechanisms and 2) until recently, GaAs has been used mostly at room temperature, where polar optic phonon scattering is much more important, and so acoustic phonon scattering has not been studied in detail. The realization of modulation doped heterostructures,[11] which significantly increase the advantages of low temperature operation of devices, has resulted in an increased interest in acoustic phonon scattering. In this work we will focus on acoustic deformation potential scattering in

modulation doped $Al_xGa_{1-x}As$/GaAs heterostructures. The wave function of the electrons in these structures is confined mostly to the GaAs, and we expect the relevant deformation potential constant to be that of GaAs.[12] We therefore start with a brief review of previous measurements of Z in bulk GaAs.

2.2. Previous Measurements of Z in Bulk GaAs

There have been a number of studies of the deformation potential constant in GaAs, and the reported values of Z range from 6 eV to 16.8 eV.[13-22] Obviously, some of these measurements have been dominated by spurious effects. It is often difficult to determine from the published reports which experiments are the most accurate, but there is a simple way to determine an upper bound for the value of the deformation potential, as suggested by Walukiewicz.[23]

The major scattering mechanisms in bulk GaAs at 77 K are deformation potential scattering, polar optic phonon scattering, piezoelectric scattering, and impurity scattering. The first three of these are the same for all samples of GaAs, while the last depends on the doping level and the compensation ratio. We have calculated an upper limit to the mobility in bulk GaAs at 77 K including only the first three scattering mechanisms for various values of the deformation potential constant. The mobility was calculated using the iterative procedure of Rode[24] to solve the Boltzman equation for low applied fields.[25] A deformation potential of 16 eV (a commonly cited number) limited the mobility to approximately 116 000 $cm^2\ V^{-1}\ s^{-1}$, considerably below the observed maximum of approximately 210 000 $cm^2\ V^{-1}\ s^{-1}$. The observed maximum mobility is reached with a deformation potential of 11 eV, but this is without the effects of impurity scattering,

which can be significant. We can therefore be confident that the true deformation potential constant of GaAs is somewhat less than 11 eV. With this in mind, we consider the measurements of Z in bulk GaAs.

In bulk GaAs, the deformation potential constant has most commonly been determined by adjusting Z to give the best fit between theoretical calculations of the mobility and experimental measurements. The theoretical calculations must include the contributions from all scattering mechanisms, and any error in estimating the contributions of the other mechanisms will increase the error in the value of the deformation potential constant that is determined. The most accurate experiments are those that are designed to minimize the relative contributions of the additional scattering mechanisms, and to accurately estimate whatever contributions remain.

The most difficult scattering mechanism to account for is that of impurity scattering. In the temperature range over which the total mobility is most sensitive to the value of the deformation potential constant (roughly 45 K to 85 K) both ionized impurity and neutral impurity scattering are important. The donor concentration N_d and the acceptor concentration N_a must be known if these scattering mechanisms are to be accounted for. It has been shown[26] that N_d and N_a can be calculated from the temperature dependence of the electron concentration if the sample is lightly doped (so that carrier freeze-out is observed) or from the temperature dependence of the mobility otherwise. The measurement of N_d and N_a is most accurate when the data covers a large range of temperatures, typically 4 K to 400 K.

Lightly doped samples are most suitable for determinations of the deformation potential because they have reduced impurity scattering, which makes deformation

potential scattering relatively more important, and because N_d and N_a can be more accurately determined from carrier freeze-out than from the temperature dependence of the mobility. However, it is difficult to grow high purity GaAs, and as a result there are a number of studies of relatively impure samples. It is these studies of relatively low mobility samples that have reported the largest values of the deformation potential constant.

The study by Wolfe et al.[13] reported measurements of high mobility samples, and is therefore the least likely to overestimate the value of the deformation potential constant. The total impurity concentration $N_d + N_a$ was less than 2×10^{14} cm^{-3} for all of their samples, and the mobility at 77 K was as high as 210 000 cm^2 V^{-1} s^{-1}. The impurity concentrations were determined from the temperature dependence of the electron concentration, and the deformation potential constant was adjusted to produce the best fit between the theoretically predicted mobility and the measured mobility. Figure 2.1 reproduces their graph of the temperature dependence of the various scattering mechanisms along with experimental data from a high mobility sample and the best fit of the total mobility. Note that deformation potential scattering is an important scattering mechanism in bulk GaAs only over a limited temperature range. They found that a 10% variation in the deformation potential constant produced a 5% variation in the total mobility for temperatures between 45 K and 85 K. This sensitivity to the deformation potential constant is found only in high purity samples with minimal impurity scattering.

A deformation potential of 7.0 eV was necessary to fit their data. This measurement could be anomalously low if the true mobility were actually lower, or if the impur-

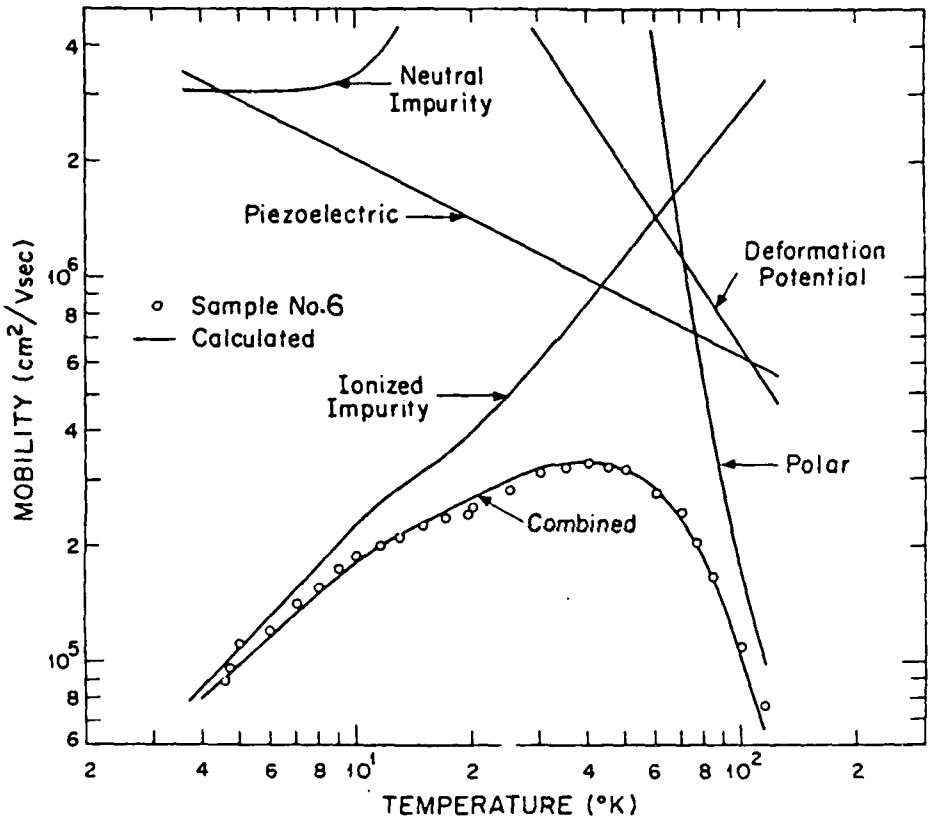

Fig. 2.1. A graph of the experimentally measured mobility in a high mobility bulk GaAs sample, the calculated contribution of each scattering mechanism to the total mobility, and the best fit of the calculated mobility to the data. The deformation potential constant necessary to produce the best fit was 7.0 eV. The impurity concentrations N_a and N_d were determined from the temperature dependence of the electron concentration. Note that deformation potential scattering makes a significant contribution over a limited range from about 45 K to 85 K. Although deformation potential scattering can become important at high temperatures, the conduction in the L and X valleys complicates the interpretation of data and makes a determination of the deformation potential constant difficult. Reproduced from Reference 13.

ity levels were overestimated. A number of studies have measured mobilities of around 200 000 $cm^2 V^{-1} s^{-1}$ at 77 K, and it is unlikely that this is a source of error. Although an overestimate of the impurity scattering would result in an anomalously low value for the deformation potential constant, the measured mobility still sets an upper limit of 11 eV, as discussed earlier.

Other values which have been reported in the literature include 6.0 eV, determined from free carrier absorption,[17] 6.3 eV, also determined from free carrier absorption,[16] 7.0 eV, estimated from the pressure dependence of the band gap,[19] 9.3 eV, determined from the pressure derivative of transition metal defects,[20] 11.5 eV, extrapolated from trends observed in other compounds, primarily ZnSe,[15] 15.7 eV, determined from free carrier absorption,[21] 16.0 eV, determined from the mobility in doped samples at high temperatures,[14] and 16.5 eV, from an unspecified method.[18] A number of these studies choose a value for the deformation potential constant without presenting any data to substantiate the result. The larger values have generally been reported in studies which used less reliable methods of measurement, as we would expect from our discussion of the upper limit.

2.3. Previous Measurements of Z in Heterostructures

The low temperature mobility of a modulation doped heterostructure is more sensitive to the deformation potential constant than the mobility of a bulk sample. This is because the reduction in impurity scattering which accompanies modulation doping increases the relative importance of phonon scattering. Phonon scattering is particularly important at the low temperatures where impurity scattering would dominate in bulk samples.

The wave function of an electron in a $Al_xGa_{1-x}As/GaAs$ modulation doped structure is confined almost entirely to the GaAs, and we expect the scattering to depend on the deformation potential of the GaAs. However, a number of studies of acoustic deformation potential scattering in $Al_xGa_{1-x}As/GaAs$ heterostructures have suggested a deformation potential constant of 11 eV to 16 eV, [27-33] considerably larger than the accurate values for bulk GaAs.

Most of the studies of the deformation potential in heterostructures have been based on the temperature dependence of the mobility,[27-32] and they suffer from the same difficulty as the studies in bulk GaAs, namely the uncertainty in the contributions from mechanisms other than deformation potential scattering. In heterostructures there are scattering mechanisms not present in bulk material, such as interface roughness scattering, and they have not been quantitatively characterized. The calculation of impurity scattering is more complicated than in bulk material because it must include both the local background impurities in the bulk GaAs and the remote donors in the $Al_xGa_{1-x}As$. The background impurity level is difficult to measure experimentally because it is small compared to the electron concentration and there is no carrier freeze out. The remote impurity scattering is difficult to predict theoretically because of its sensitivity to the impurity potential and wave function of the electron. As a result, it is not possible to theoretically predict the total mobility with enough accuracy to deduce a deformation potential. Efforts have been made to circumvent this problem by analyzing the temperature dependence of the mobility.

Although the absolute mobility cannot be computed accurately, Price has proposed that the temperature dependence can.[34] He has suggested that at temperatures below

40 K the impurity scattering rate is independent of temperature and that the sole source of the temperature dependence of the mobility is acoustic phonon scattering. If correct, this eliminates the need to understand the details of impurity scattering. The theory of acoustic phonon scattering then predicts that the slope of the temperature dependence of the mobility will depend directly on the deformation potential. Of course, if other temperature dependent scattering mechanisms contribute to mobility then the deformation potential constant determined from these experiments will be inaccurate.

Lin et al. have reported a comprehensive study of the temperature dependence of the mobility in modulation doped $Al_xGa_{1-x}As/GaAs$ heterostructures.[30] They measured the temperature dependence of the resistance in a set of modulation doped single heterostructures that exhibited a wide range of mobilities. The electron concentration in their samples was independent of temperature, and so the temperature dependence of the resistance was the same as the temperature dependence of the inverse mobility. Figure 2.2 is reproduced from their paper, and shows the temperature dependence of the resistance normalized to the extrapolated zero temperature resistance. The low mobility samples (which had a large impurity scattering rate) exhibited a negative temperature coefficient of the inverse mobility. This is easily explained as being due to the temperature dependence of the impurity scattering. Samples with high mobilities (and corresponding low impurity scattering rates) have a temperature coefficient with the opposite sign. They interpret this as indicating that the temperature dependence of the impurity scattering is insignificant in the high mobility samples. Based on this interpretation, they deduce a deformation potential constant of 13.5 eV from the temperature dependence of the mobility in their high mobility samples. This is in agreement with the value that Men-

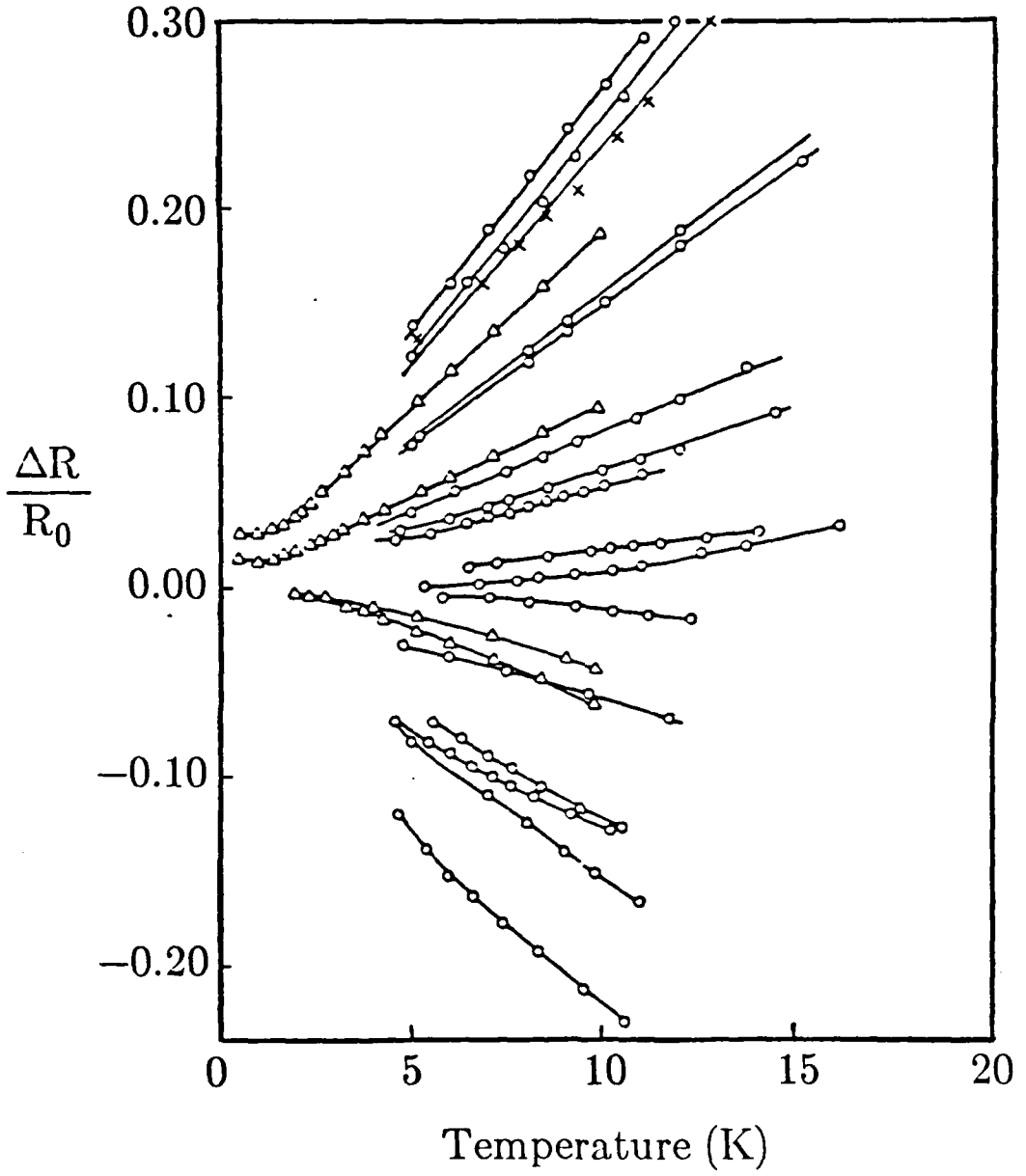

Fig. 2.2. The variation of resistance (proportional to inverse mobility) in a set of samples with different low temperature mobilities. The samples with low mobilities (as low as 20 000 $cm^2\ V^{-1}\ s^{-1}$) are at the bottom of the graph, and show a negative temperature coefficient of resistance typical of impurity scattering. The highest mobility samples (up to 200 000 $cm^2\ V^{-1}\ s^{-1}$) show a positive temperature coefficient of resistance, which Lin et al. interpret as being due solely to deformation potential scattering. Intermediate mobility samples show intermediate temperature coefficients. Reproduced from Reference 30.

dez et al. found in a less comprehensive study of a single high mobility sample.[27] Other studies based on the temperature dependence of the mobility have also reported values ranging from 11 eV to 14 eV.[31,32]

2.4. Power Loss Through Deformation Potential Scattering

The discrepancy between the measured value of Z in the $Al_xGa_{1-x}As$/GaAs heterostructure and the value in bulk GaAs suggests that there may be additional scattering mechanisms which affect the temperature dependence of the mobility in the heterostructure. This is of particular concern since Lin et al. found in their study samples for which other scattering mechanisms were of demonstrable importance. This possibility is inherent in any measurement which depends on the mobility, because the mobility is determined by the combination of all scattering processes. In our study of the deformation potential constant we measure the power loss of the conduction electrons and vary Z to fit the theoretical power loss to our experiment. The power loss is of course independent of elastic scattering mechanisms such as impurity scattering or interface roughness scattering. Thus, the measurement of Z from the power loss requires fewer assumptions about the types of scattering mechanisms present and is potentially more reliable. This method was originally developed to investigate scattering mechanisms in silicon inversion layers.[35]

In the next chapter we explore the problems inherent in a calculation of the power loss (most of which are common to the calculation of the mobility) and outline our calculation, which must be done by numerical integration on a computer.

3. THEORY OF THE POWER LOSS

3.1. Introduction to the Method

Our determination of the deformation potential constant involves two parts: the theoretical calculation of the power loss, and the experimental measurement of the power loss in terms of the variables used in the theoretical calculation. In this chapter we discuss the theoretical calculations, first describing the general approach and the independent variables on which the power loss depends, and then deriving the equation for the power loss. The variables of the power loss equation are the quantities which we measure experimentally. In the last part of this chapter we discuss and compare both analytical and numerical solutions for the power loss equation.

We calculate the transport properties using a semiclassical approach. The Schrödinger equation for the electron–lattice system is first simplified by making the adiabatic approximation, which separates the equations of motion for the electrons and the atoms. Phonons are then treated as perturbations which cause the electrons to make transitions between states. The effective mass theorem simplifies the equation of motion further and allows us to calculate the wave functions of the electrons. This calculation is complicated considerably by the confinement of the electrons at the heterointerface, an important problem which we will return to later. With these approximations we then use a method based on the Boltzman transport equation to determine the electron distribution function necessary to balance the power lost to phonon emission with the power gained from the electric field.

The Boltzman equation approach requires a calculation of the effect of collisions on the distribution function of the electrons. We use Fermi's golden rule to calculate the

rate at which the perturbing potential of the acoustic phonons causes transitions of electrons between states. We must verify that Fermi's golden rule is applicable to the conditions of our experiment. Peierls has pointed out that in a degenerate system the scattering time τ and the Fermi energy ϵ_f must satisfy the inequality $\tau\epsilon_f > \hbar$ if the electrons are to be in well–defined states, which is, of course, an important assumption of our approach.[36] The Fermi energy of our samples is of the order of 15 meV, and we infer from the mobility a τ of approximately 1×10^{-12} s, which easily satisfies this inequality. Note also that the mean free path of an electron is longer than its de Broglie wavelength, which is necessary if we are to assign a wavelength to the electron.

3.2. The Independent Variables

Given the validity of the semiclassical approach we can easily calculate the phonon induced rate of transitions between electron states. The power loss is then calculated by averaging the transition rates, weighted by the energy gained or lost, over the occupied electron states. Our calculation of the matrix elements for transitions depends on the available phonon modes, their occupation numbers, and the wave function of the electron. The average of the transition rates over the occupied electron states depends on the distribution function for the electrons. The independent variables in our calculation of the power loss depend on our assumptions regarding these parameters.

In our work we adopt the assumption that the phonon modes are those of bulk GaAs. That is, we ignore perturbations of the phonon modes caused by the difference in the elastic constants of the GaAs and the $Al_xGa_{1-x}As$, and we ignore perturbations of the modes caused by the close proximity of the crystal surface. This may be an oversimplification. It seems probable that long wavelength phonons will be affected by

the proximity of the surface of the crystal. Mendez et al.[27] justify the assumption of bulk phonon modes by citing magnetophonon experiments which indicate that the energy of the polar optical phonon modes is relatively unchanged, but this energy is probably insensitive to the mode of the phonon, and therefore a poor indicator of any disturbance in the modes. Interface phonons have been clearly observed in $Al_xGa_{1-x}As/GaAs$ superlattices,[37] but we know of no conclusive work on single heterojunctions. Studies of the mobility in single heterojunction silicon Metal Oxide Semiconductor Field Effect Transistors (MOSFET) inversion layers have shown that interface modes can be important in that system,[38-40] but this result is not directly comparable to the $Al_xGa_{1-x}As/GaAs$ system because the elastic constants of $Al_xGa_{1-x}As$ and GaAs do not differ as much as do those of Si and SiO_2. We continue with the assumption of bulk 3D phonon modes because there exists no definitive theory of interface modes.

The occupation numbers of the phonon modes are assumed to be given by the Planck distribution function, characterized by the lattice temperature T_l. Of course, power loss from the electrons is accomplished by emitting phonons, which will change the occupation numbers of the phonon modes. The excess heat of the emitted phonons is absorbed by the surrounding system, which in our experiment is a liquid helium bath. At the low levels of excitation in our experiment the rate at which energy is transferred to the helium bath is much greater than the rate at which the electrons transfer energy to the lattice, and it is not necessary to consider hot phonon effects.

The energy of the phonon modes is determined from the linear dispersion relation, $\hbar\omega_Q = \hbar u Q_3$, where ω_Q is the phonon frequency, Q_3 is the three-dimensional phonon wave vector, u is the speed of sound, and $\hbar$ is Planck's constant. This dispersion relation

should be quite accurate for the long wavelength phonons which are excited at the low temperatures of our experiment.

It is more difficult to determine the correct electron distribution function to use in our calculations. The applied electric field disturbs the distribution function from its equilibrium values, and an exact calculation of it would require a solution of the Boltzman transport equation that included all the scattering mechanisms, which is difficult and unnecessarily complicated for our purposes. However, under the limited conditions of our experiment the distribution function can be accurately approximated.

The electron–electron interaction exchanges energy and momentum between electrons without changing their total energy, and it will tend to drive the electrons into equilibrium with themselves. Other mechanisms, such as acceleration by an electric field or emission of phonons, add or remove energy from the electrons and drive the distribution away from equilibrium. If the electron–electron scattering rate is much larger than the phonon emission rate, then the electrons will very nearly be in equilibrium with themselves, and they will be characterized by a Fermi–Dirac distribution function $f(\epsilon)$ with an elevated electron temperature T_e and a Fermi energy ϵ_f.[41] An electric field will cause T_e to increase until the power lost to phonon emission balances the power input from the electric field.

A number of studies have investigated the conditions necessary for the hot electron model to be valid. The important requirement is that the electron–electron scattering rate exceeds the net phonon emission rate. Electron–electron scattering increases with increasing electron density, and phonon emission increases with increasing electron temperature. For given electron and lattice temperatures, there is a minimum density of

electrons for which the hot electron model will be valid. A review by Ferry[42] suggests that a bulk electron concentration of 10^{16} cm^{-3} would be adequate for the conditions of our experiment. A bulk density of 10^{16} cm^{-3} corresponds to a two–dimensional electron gas density of approximately 5×10^{10} cm^{-2}. The density of electrons in our experiment is an order of magnitude larger than this, and we expect the electron temperature model to be valid. Preliminary studies of the distribution function through Monte Carlo simulations of a two–dimensional electron gas in an $Al_xGa_{1-x}As/GaAs$ heterostructure confirm this estimation.[43]

Finally, the matrix element for phonon interactions depends on the wave function of the electron. In a heterojunction, the calculation of the wave function of the electrons is complicated by potentials which confine the electron near the heterointerface. These potentials cannot be treated as perturbations because they do more than cause transitions between existing states – they change free states to bound states. This change is at the heart of many of the interesting phenomena observed in heterojunctions. It is also the cause of many of the difficulties in calculations of the properties of the heterojunction.

The important potentials are those of the band gap discontinuity at the heterojunction, the electrostatic potential as determined from Poisson's equation (where the charge is that of the ionized donors and acceptors plus that of the free carriers), and refinements such as the exchange–correlation potential and the image force potential. These refinements are sometimes ignored in order to get simple analytic solutions for the wave functions. The wave functions are determined by solving the time–independent Schrödinger equation

$$\left[-\frac{\hbar^2}{2m^*}\nabla^2 + V(z)\right]\psi = E\psi, \tag{3.1}$$

where V(z) is the potential and the remaining symbols have their usual meanings. We assume that the crystal structure and doping is a function of the z coordinate only. Note that an exact solution of this equation requires that the potential due to the electrons be included self–consistently in V(z).

This equation may be separated into the part dependent on the coordinates parallel to the heterojunction (x and y) and the part dependent on the coordinate perpendicular (z.) The envelope wave function of the electron is then given by

$$\psi = e^{i\mathbf{k}\cdot\mathbf{r}}\phi_n(z), \tag{3.2}$$

where $\mathbf{k}$ is the wave vector of the electron in the xy plane, $\mathbf{r}$ is a two–dimensional vector in the xy plane, and $\phi_n(z)$ is a solution of

$$\left[\frac{-\hbar^2}{2m^*}\frac{\partial^2}{\partial z^2} + V(z)\right]\phi_n = E_n\phi_n. \tag{3.3}$$

The calculation of the scattering rate (and hence the transport properties) now requires an evaluation of the matrix element

$$M_{nm} \propto \left\langle e^{i\mathbf{k}_f\cdot\mathbf{r}}\phi_n(z)\,|\,e^{i\mathbf{Q}\cdot\mathbf{r}}e^{iqz}\,|\,e^{i\mathbf{k}_i\cdot\mathbf{r}}\phi_m(z)\right\rangle, \tag{3.4}$$

where $\mathbf{k}_i$ is the initial wave vector of the electron and ϕ_m the initial perpendicular wave function. Similarly, $\mathbf{k}_f$ is the final wave vector and ϕ_n the final perpendicular wave function. The phonon wave vector has been divided into its component parallel to the interface, $\mathbf{Q}$, and its component perpendicular to the interface, q.

The parallel components of crystal momentum are conserved, just as they are when three–dimensional electrons scatter. However, the perpendicular components are not. Instead, the transition rate is proportional to

$$I_{nm} = \int \phi_n^*(z) e^{iqz} \phi_m(z) dz, \tag{3.5}$$

where I_{nm} is called the overlap integral or the form factor. Transitions may be between states within the same subband (n = m) or they may be between subbands (n ≠ m.) If the higher subbands have insignificant populations then it is sufficient to consider intrasubband transitions within $\phi_0(z)$. At the electron concentration and the temperatures of our experiment this is the case, and the only overlap integral we will be concerned with is $I_{00}(q)$, which we will henceforth refer to as I(q). The failure of the conservation of crystal momentum in the perpendicular direction is the result of the term V(z) in the Hamiltonian. This term breaks the translational symmetry from which the conservation of crystal momentum followed.[44]

The replacement of momentum conservation with the overlap integral makes accurate calculations of the transport properties difficult. A small change in $\phi(z)$ can result in large changes in I(q) and hence in the scattering rate. We now consider various methods of solving for $\phi_n(z)$.

The conduction and valence band discontinuities which occur at a heterojunction are an important contribution to the potential V(z). These discontinuities are necessary to accommodate the difference in the band gap energies of the materials. Because of the commercial applications of the $Al_xGa_{1-x}As/GaAs$ system there is considerable data available on it, and the band alignment has been well characterized. It is now known that approximately 65% of the band gap difference appears in the conduction band discontinuity and the remainder in the valence band discontinuity.[45] (The previously accepted value[46] of 85% is now generally considered to be in error. The error is attributed to spurious effects such as band bending, which can change the effective barrier height

measured in some experiments,[47] and to the insensitivity of the original measurements to the band edge discontinuity.[48,49]) The 65% rule results in a conduction band step of $\Delta E_c \approx 0.79x$ (eV) at the heterojunction. For the samples used in this study the discontinuity was approximately 240 meV.

The potential V(z) is complicated by the band bending due to the electrostatic potential of the donors, acceptors, and free carriers. Donors in the $Al_xGa_{1-x}As$ supply free electrons which transfer to the GaAs where the conduction band minimum has a lower energy than that of the $Al_xGa_{1-x}As$. This charge separation causes band bending, which tends to confine the electrons to the interface. An example of the resulting band structure is shown in Fig. 3.1.

If there is strong band bending, then there are a number of approximations for V(z) which allow for simple analytic solutions for the $\phi_n(z)$ with low energies. If the $Al_xGa_{1-x}As$ is strongly N type, and the GaAs is P type, then there will be a large density of transferred electrons in the GaAs and a long depletion width. The low energy electrons will be localized near the interface where the band bending is approximately linear, as shown in Fig. 3.1. It is then convenient to approximate V(z) by an infinite barrier at the heterojunction and a linearly increasing barrier in the GaAs.[50] This is the triangular well approximation.

Although $\phi_n(z)$ can be calculated exactly within the limits of the triangular potential approximation,[50] the solutions (Airy functions) are cumbersome, and not in keeping with our search for easily manipulated analytic solutions. It is generally more convenient to use a variational wave function. The most commonly used variational wave function,[50] called the Fang–Howard wave function, is

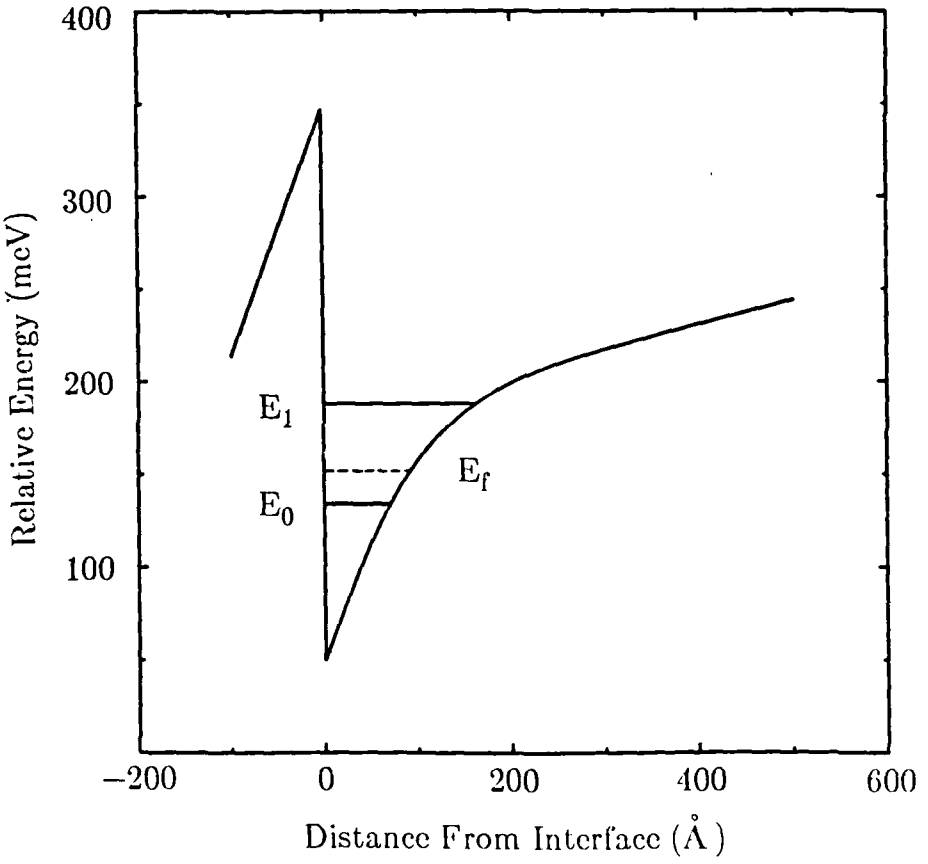

Fig. 3.1 The variation of the conduction band edge energy with distance in a modulation doped $Al_xGa_{1-x}As/GaAs$ heterojunction. Also shown are the energy levels of the first two subbands and the Fermi energy. The band bending was calculated self-consistently for a temperature of 4.2 K, an electron concentration of 5×10^{11} cm^{-2}, a GaAs background doping of $N_a - N_d = 10^{15}$ cm^{-3}, and an $Al_xGa_{1-x}As$ doping level of $N_d - N_a = 2\times10^{18}$ cm^{-3}.

$$\phi_0(z) = (\frac{b^3}{2})^{1/2} z e^{-bz/2}. \tag{3.6}$$

The variational parameter is b, and z is measured from the interface as shown in Fig. 3.1. The variational parameter is determined by minimizing the energy. If we include contributions from the kinetic energy of the electrons and the interaction energy of the electrons with the depletion charges and the other electrons, then b is given by

$$b = \left[\frac{48\pi m^* e^2 \left(\frac{11}{32} N_s + N_{depl} \right)}{\epsilon_r \epsilon_0 \hbar^2} \right]^{1/3} \tag{3.7}$$

where N_s is the two–dimensional density of electrons, N_{depl} is the product of the acceptor density in the GaAs and the depletion width, ϵ_r is the relative low frequency dielectric constant, and ϵ_0 is the permittivity of free space. Although this wave function is quite convenient because of its simplicity, it is of limited accuracy in GaAs.

The triangular well approximation and the variational wave function were originally developed to describe the electrons in inversion layers of silicon MOSFETs. These approximations are considerably less accurate in $Al_xGa_{1-x}As/GaAs$ heterojunctions. The approximation of an infinite barrier at the heterojunction is less accurate in $Al_xGa_{1-x}As/GaAs$ heterojunctions, where the discontinuity is of the order of 0.3 eV, than it is in a Si/SiO_2 heterojunctions, where the discontinuity is about 3.0 eV. In addition, the lower effective mass of electrons in GaAs results in a wave function with a larger spatial extent, which reduces the accuracy of the linear approximation for the band bending potential.

The most accurate model of electrons at $Al_xGa_{1-x}As/GaAs$ heterojunctions is one which numerically calculates self–consistent values for V(z) and $\phi_n(z)$. This allows us to

replace the infinite barrier used for the variational wave function with an accurate barrier height, and it allows the inclusion of second–order effects such as the exchange–correlation potential, which cannot be included in analytic models. The self–consistent wave function is calculated iteratively, assuming a potential, calculating the wave function, using the wave function to calculate the new potential, and then repeating until the calculation converges.[51] Although the self–consistent wave function requires numerical calculation of the transport properties, it is significantly more accurate than the variational wave function, and it is necessary for an accurate analysis of experimental data.

In Fig. 3.2 we compare the wave function for a single $Al_xGa_{1-x}As/GaAs$ heterojunction as calculated using both the Fang–Howard variational model and the self–consistent numerical model. The self–consistent calculation shows that the true wave function has a significant extent into the $Al_xGa_{1-x}As$, which the variational wave function cannot reproduce. This extension into the $Al_xGa_{1-x}As$ has a significant effect on the potential and the wave function because of the interaction of the electrons with the positively charged donors in the $Al_xGa_{1-x}As$, and this changes the overlap integral.

In Fig. 3.3 we compare the overlap integral as calculated from both the variational and the self–consistent wave functions. There are significant differences at the phonon wave vectors which are important to our calculation of the power loss. The use of the variational wave function would therefore introduce a large error into our calculations.

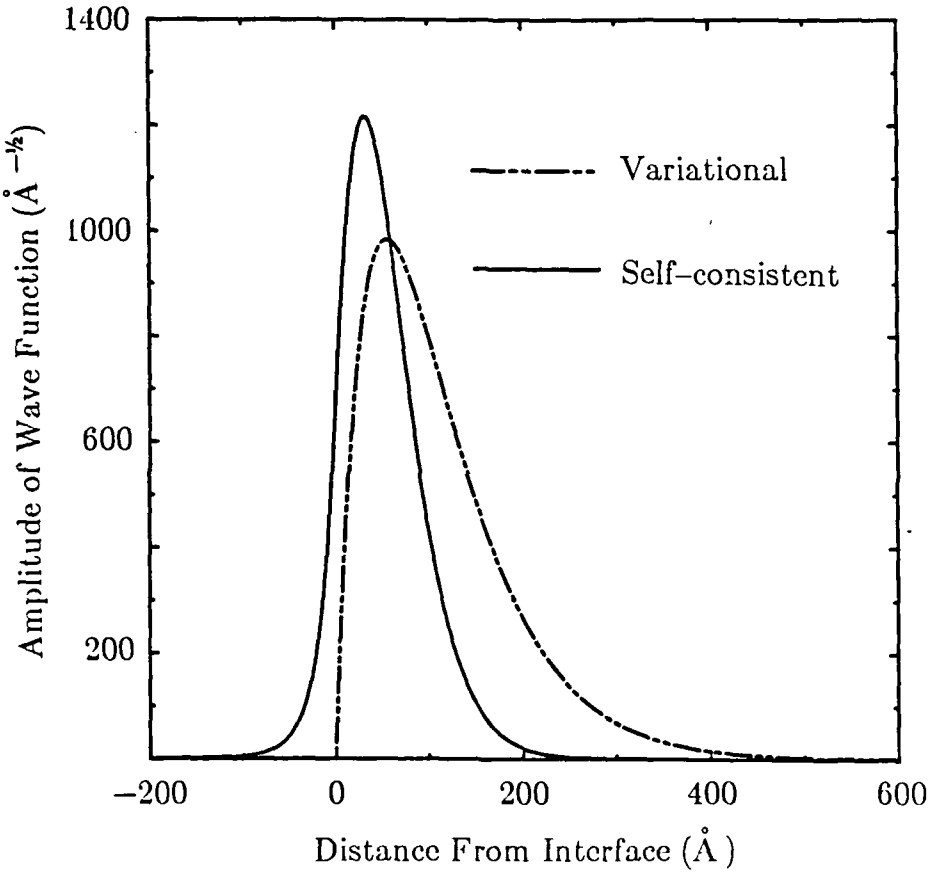

Fig. 3.2 A comparison of the self–consistent and the variational wave functions. The self–consistent wave function was calculated for a barrier height of 240 meV, while the variational wave function assumes an infinite barrier. The majority of the difference between the two wave functions is caused by the interaction of the self–consistent wave function with the positively charged donors in the $Al_xGa_{1-x}As$. The variational parameter was calculated from Eq. (3.7) using a depletion width of 1.3 μm. The doping levels and sheet carrier concentrations are the same as those used for Fig. 3.1.

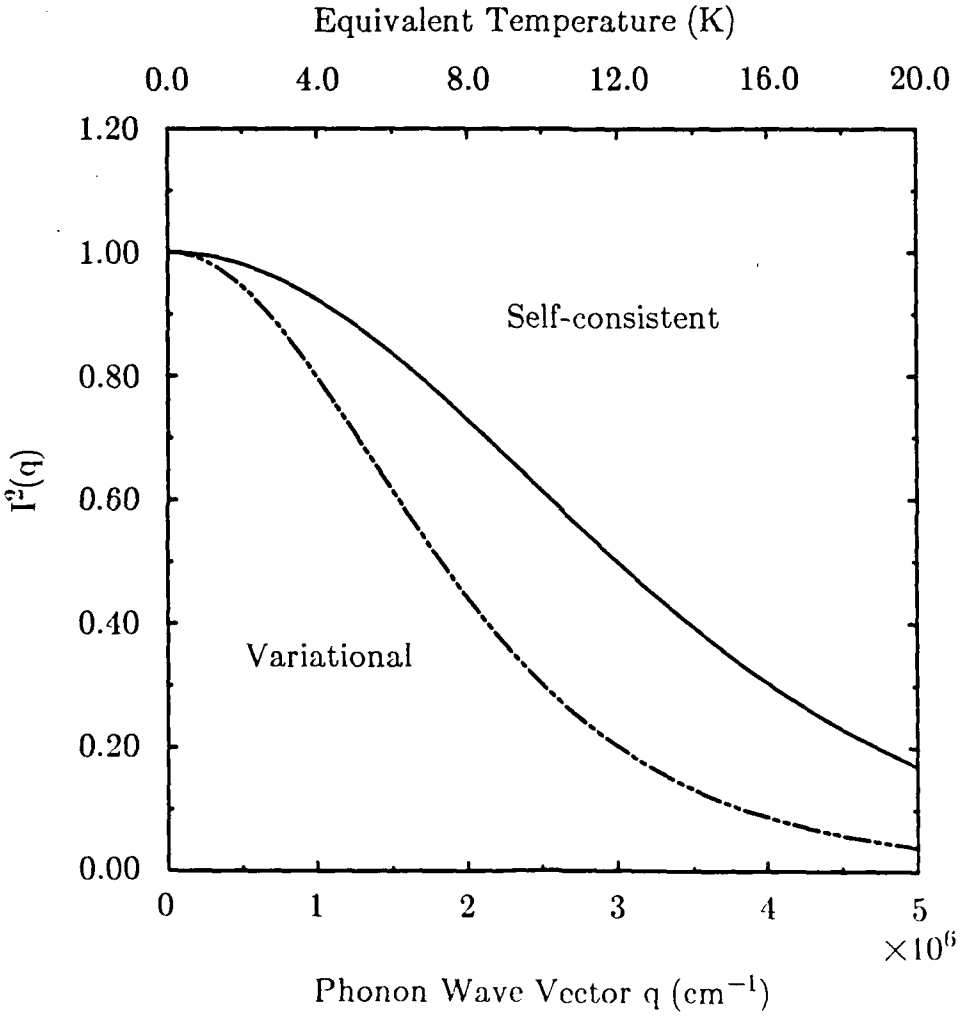

Fig. 3.3 A comparison of the overlap integral calculated from the self-consistent wave function with the overlap integral from the variational wave function. Computed using the wave functions shown in Fig. 3.2. The equivalent temperature is defined by $kT = \hbar u_l q$.

3.3. Screening of the Electron–Phonon Interaction

In bulk GaAs the screening of the acoustic phonon interaction has generally been ignored. At the high electron densities where screening of the acoustic phonon interaction would be important the mobility is dominated by impurity scattering, while at low electron densities the screening is not significant. Modulation doped heterostructures combine minimal impurity scattering with the high electron densities necessary for effective screening, and the possible effects of this screening must be investigated. However, different researchers have reached different conclusions on the importance of screening. Walukiewicz has found good agreement with experimental data using a theory which does not include screening,[23,52] while Price finds that screening must be included.[29] We consider both the theory without screening and the theory with screening, and we discuss a simple experimental method to determine which one is applicable.

The matrix element for the screened interaction is given by the matrix element for the unscreened interactions multiplied by a screening factor. Following Price,[53] we use a screening factor calculated using the Lindhard theory of the dielectric function and considering only static potentials. The Lindhard theory is appropriate for small potentials which produce a linear response, and is essentially valid for the potentials of acoustic phonons. The static screening factor is accurate for potentials which vary slowly in time, and is appropriate for the low frequency phonons excited at the temperatures of our experiment. At high temperatures it may be necessary to use a more sophisticated theory of screening. With these approximations the screening factor is given by[53]

$$S(Q) = \frac{Q}{Q + PH(Q)}, \tag{3.8}$$

where H(Q) is

$$H(Q) = \int\int \phi(z_1)\phi(z_2)\exp(-Q\,|z_1-z_2\,|)dz_1dz_2, \tag{3.9}$$

and P is a constant characteristic of the material,

$$P \cong \frac{2m^*e^2}{\epsilon_r\epsilon_0\hbar^2}. \tag{3.10}$$

For the effective mass and dielectric constant of GaAs, $P = 2\times10^6$ cm^{-1}.

These equations describe the effects of the polarization of a two–dimensional electron gas within a subband. They do not include the screening effects related to intersubband transitions, which are not expected to be important under the conditions of our experiment.[53]

Our experimental data is analyzed using a screening factor computed without further approximation from Eqs. (3.8) and (3.9), including the self–consistent electron wave functions, but in some applications a simplified expression for an approximate screening factor is useful and accurate. For small Q, H(Q) approaches unity, and if $Q \ll P$ then the screening factor approaches

$$S(Q) = Q/P. \tag{3.11}$$

This is the strong screening approximation. We use the approximation later in our analytic solution of the power loss equation, and we discuss its accuracy in more detail then.

Screening of the scattering potential changes the Q dependence of the matrix element, and this changes the temperature dependence of the power loss. Hence it is in principle possible to determine experimentally the importance of screening by measuring the temperature dependence of the power loss. We will discuss this further in the section on analytic solutions of the power loss.

3.4. The Power Loss Equation

Our goal is to calculate the power loss as a function of the parameters discussed in the previous section: the lattice temperature T_l, the electron temperature T_e, the Fermi energy ϵ_f, and, indirectly, the wave function of the electron. The power loss is normally calculated from the third moment of the Boltzman transport equation. This approach is outlined in standard texts on semiconductors,[54] and it is easily modified to include our assumption that the effect of the electric field on the distribution function is to increase the characteristic temperature of the Fermi–Dirac distribution function. Here we will follow instead a slightly different approach described by Conwell.[55] It is entirely equivalent to taking the moment of the Boltzman equation, but it perhaps makes clearer the physical meaning of the various terms, and it is more easily extended to include the effects of disturbed phonon modes or hot phonon effects.

We start by calculating the time rate of change of the phonon distribution function N_Q as caused by phonon emission and absorption. This is just the difference between the transition rate for phonon emission and absorption from a particular electron state summed over all filled electron states and is given by

$$\frac{\partial N_Q}{\partial t} = 2\frac{2\pi}{\hbar}\sum_{\mathbf{k}} S^2(Q)I^2(q)M^2(Q)\,\delta(\epsilon_k+\hbar\omega_Q-\epsilon_{k+Q}) \times \{(N_Q+1)f(\epsilon_{k+Q})[1-f(\epsilon_k)] - N_Q f(\epsilon_k)[1-f(\epsilon_{k+Q})]\}. \tag{3.12}$$

The initial factor of 2 is for the spin degeneracy of the electrons, the summation is over the two–dimensional electron wave vector, ϵ_k and ϵ_{k+Q} are energies defined by $\epsilon_x = \frac{\hbar^2 x^2}{2m^*}$, $\delta(x)$ is a Dirac delta function, and f(E) is a Fermi–Dirac function characterized by a Fermi energy ϵ_f and an elevated electron temperature T_e. The unscreened theory is

obtained by setting S = 1. Here Q_3 is the three–dimensional phonon wave vector, Q is the component of Q_3 parallel to the heterointerface and q is the component perpendicular. Although it is not entirely consistent with our definitions of Q_3, Q, and q, we have maintained tradition in using N_Q for the function describing the occupation numbers of the three–dimensional phonons and ω_Q for the frequency of the three–dimensional phonon. On the right–hand side of the above equation we take N_Q to be given by the Planck distribution function. If we were to include hot phonon effects we would combine our calculation of $\partial N_Q/\partial t$ with an equation for the decay of the hot phonons in order to determine more exactly the correct form for N_Q on the right–hand side. As stated earlier, we neglect hot phonon effects because they are of minimal importance under the conditions of our experiment.

The matrix elements M(Q) are given by

$$M^2(Q_3) = \frac{Z^2 \hbar Q_3}{2\rho u_l} \tag{3.13}$$

for deformation potential scattering,

$$M^2(Q_3) = \frac{\hbar (eh_{14})^2}{2\rho u_l} \frac{9q^2Q^4}{2Q_3^7} \tag{3.14}$$

for longitudinal piezoelectric scattering, and

$$M^2(Q_3) = \frac{\hbar (eh_{14})^2}{2\rho u_t} \frac{8q^4Q^2 + Q^6}{2Q_3^7} \tag{3.15}$$

for transverse piezoelectric scattering.[56] The longitudinal and transverse sound velocities are given by u_l and u_t, respectively, ρ is the density of the crystal lattice, and eh_{14} is the piezoelectric constant. The remaining symbols have their usual meanings.

Using the net rate of phonon emission we calculate the average power loss per electron as

$$<\frac{\partial \epsilon}{\partial t}> = \frac{-1}{n}\sum_{Q,q}\hbar\omega_Q \frac{\partial N_Q}{\partial t}, \tag{3.16}$$

where n is the electron concentration and the summation is over all phonon modes. After considerable manipulation, outlined in App. 1.1, we can reduce Eqs. (3.12) and (3.16) to

$$\begin{aligned} <\frac{\partial \epsilon}{\partial t}> = \frac{2u\sqrt{2m^*}}{\hbar\epsilon_f(2\pi)^2}\int_0^\infty dQ_3\, Q_3^2 \left[\exp(\hbar\omega_Q/kT_l)\exp(-\hbar\omega_Q/kT_e) - 1\right] N_Q \\ \times \int_0^{\pi/2} d\theta\, S^2(Q)\, I^2(q)\, M^2(Q_3) \\ \times \int_{\epsilon_{min}}^\infty d\epsilon_k\, \epsilon_k^{-1/2}\left[1 - \frac{(\hbar\omega_Q - \epsilon_Q)^2}{4\epsilon_k\epsilon_Q}\right]^{-1/2} f(\epsilon_k)[1 - f(\epsilon_k + \hbar\omega_Q)], \end{aligned} \tag{3.17}$$

where θ is defined such that $q = Q_3\sin\theta$ and $Q = Q_3\cos\theta$, u is either the longitudinal or transverse sound velocity, depending on which matrix element is used, and ϵ_{min} is the minimum electron energy allowed by conservation of energy and the parallel component of the wave vectors, defined as

$$\epsilon_{min} = \frac{(\hbar\omega_Q - \epsilon_Q)^2}{4\epsilon_Q}. \tag{3.18}$$

Generally it will be necessary to solve Eq. (3.17) numerically, and this is what we do for the comparison with our experiment. Each of the three integrals is computed using Simpson's rule for numerical integration. The integration to infinity over the phonon wave vector is terminated once the integrand becomes insignificant. For large phonon wave vectors the integrand decreases exponentially because of the form of N_Q, so this is a good approximation. Similarly, the integrand decreases exponentially for electron ener-

gies far from the Fermi energy, and the integration over electron energy is also terminated for very large or small energies. The integral over electron energy contains an integrable singularity at the lower limit (it goes as $\int x^{-1/2} dx$). The numerical calculation in this region requires some care if the results are to be accurate. We use a dynamically chosen variable spacing between integration points to give good resolution in the region where the integrand varies rapidly while retaining large spacing and high speed in the regions where it varies only slowly. The program is designed to have a precision of at least 1%, which is better than the experimental data to which we compare it.

3.5. The Analytical Solution of the Power Loss Equation

For the purpose of our experiment it was necessary to calculate the power loss numerically to achieve the desired accuracy. However, with some approximations, it is possible to solve Eq. (3.17) analytically, and this solution provides interesting insights into the scattering mechanism. A form of the analytical solution was originally developed by Hess to explain the power loss in silicon MOSFET inversion layers.[57] An analytical solution which eliminates some of the approximations that are not appropriate to the $Al_xGa_{1-x}As/GaAs$ system has been outlined by Price.[58]

We are concerned mostly with the power loss at low temperatures, and we discuss the approximations appropriate to low temperatures. There are three major approximations. The overlap integral I(q) must be replaced by unity. This is accurate for small phonon wave vectors. The strong screening approximation, $S(Q) = Q/P$, must be used in place of the full screening function. This is accurate for large electron concentrations and small phonon wave vectors. Finally, we must approximate the phonon occupation

numbers by $N_Q = \exp(-\hbar\omega_Q/kT)$, which is accurate at low temperatures. We will discuss further the accuracy of these approximations shortly.

With these approximations and some other minor ones we can reduce Eq. (3.17) to

$$<\frac{\partial \epsilon}{\partial t}> = F(T_e) - F(T_l), \tag{3.19}$$

where

$$F(T) = \frac{6!\epsilon^2 Z^2}{\epsilon_f^2(2\pi)^2(2m^*)^{3/2}e^4\rho\hbar^2 u_l^6}(kT)^7, \tag{3.20}$$

if we substitute the matrix element for screened deformation potential scattering. (Although our approach is slightly different from that of Ref. 58, the approximations involved are identical. Note that Eqs. (33), (34), and the constant C of Ref. 58 are apparently a factor of 2 too large.) The matrix element for screened piezoelectric scattering leads to $F(T) \propto T^5$. Further details of this derivation may be found in App. 1.2.

The term $F(T_e)$ is the energy lost to phonon emission, and the term $F(T_l)$ is the energy gained through phonon absorption. Note that if $T_e^7 >> T_l^7$, then the power gained from phonon absorption is insignificant. Thus, within the limits of the approximations, the net power loss is determined almost completely by phonon emission at electron temperatures only slightly greater than the lattice temperature.

Each factor of Q in Eq. (3.17) gives a factor of T in Eq. (3.20). The parallel and perpendicular components of Q_3, $Q = Q_3\cos\theta$ and $q = Q_3\sin\theta$ each contributes a factor of T just as Q_3 would, although they generate a different numerical prefactor. The effect of factors of Q on the temperature dependence of the power loss can be exploited to determine experimentally the importance of screening. In the strong screening approximation the screening introduces a factor of Q^2 in Eq. (3.17) and a factor of T^2 in Eq. (3.20). For

deformation potential scattering, with a matrix element $M(Q) \propto Q_3$, the power loss is then proportional to $T_e^7 - T_l^7$ if screening is important, and to $T_e^5 - T_l^5$ if it is not. The matrix element for piezoelectric scattering is proportional to $1/Q$, and the power loss to either $T_e^5 - T_l^5$ or $T_e^3 - T_l^3$, depending on the screening. Within the temperature range where the approximations are accurate the effects of screening will be clearly reflected in the temperature dependence of the power loss. The equations for the mobility are essentially the same as those for the power loss, and the mobility will show the same temperature dependencies.

Because of the difference of T^2 in the power loss of deformation potential and piezoelectric scattering they each dominate within a different temperature range. Deformation potential scattering is important at high temperatures, and piezoelectric at low temperatures, with a crossover somewhere between 1 K and 2.5 K, depending on the value of the deformation potential constant.

These simple temperature dependences are obtained only when the approximations necessary for the analytic solution are accurate. The accuracy of these approximations depends on both the electron concentration and the wave number. To illustrate the approximations, we have computed the overlap integral and the screening function using the Fang–Howard variational wave function discussed earlier. The variational parameter b was calculated for a depletion density of 0. This approximate wave function is accurate enough for the purpose of illustrating the approximations. Figure 3.4 shows the overlap integral, computed for three different electron densities, and Fig. 3.5 shows the ratio of the exact screening function to the strong–screening approximation, also for three

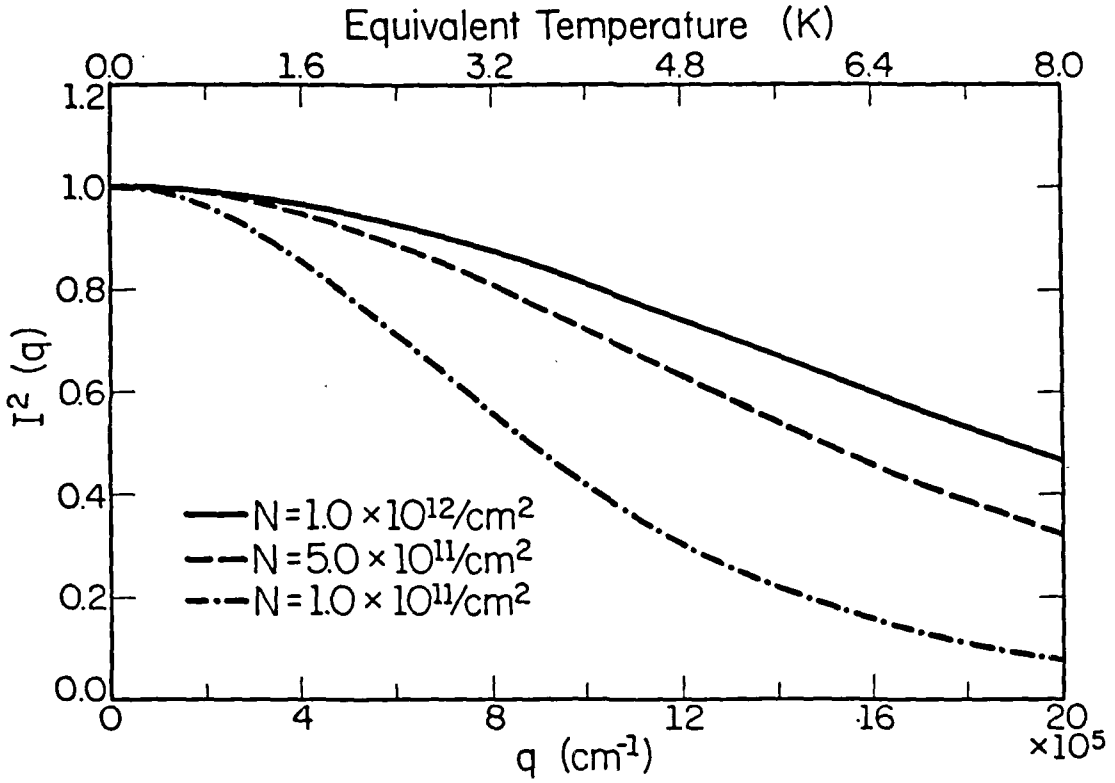

Fig. 3.4 The overlap integral as a function of q and as a function of equivalent temperature, defined by $kT = \hbar u_l q$. An equivalent temperature calculated using the transverse sound velocity would be 40% smaller. Phonons with an equivalent temperature up to an order of magnitude larger than the electron temperature contribute significantly to scattering, as discussed in the text. These curves were calculated using variational wave functions for purposes of illustration.

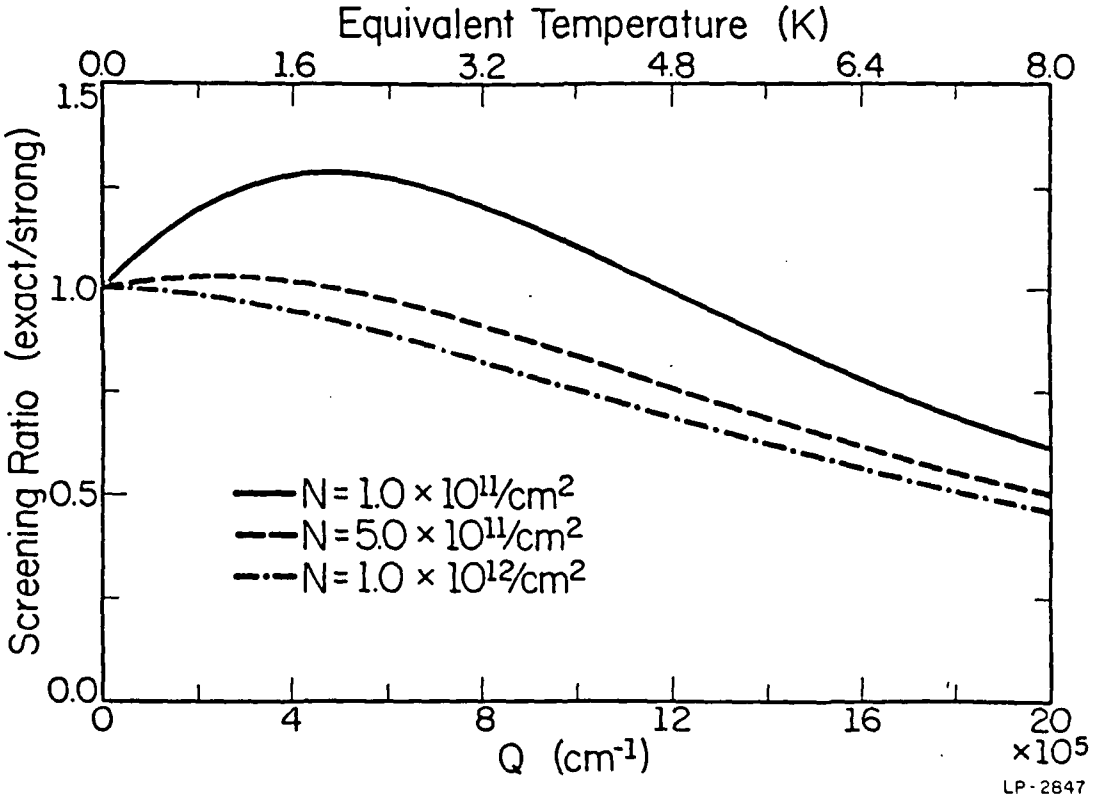

Fig. 3.5 The ratio of the exact screening function to the strong–screening approximation as a function of Q and as a function of equivalent temperature. Calculated using variational wave functions.

electron densities. It can be seen that the approximations are generally more accurate for large electron densities and small phonon wave numbers.

If the analytic calculation is to be accurate, then these approximations must be accurate for those phonons which dominate the average scattering rate. It has been suggested[58] that the analytical calculations become valid at temperatures for which $\hbar u k_f < kT$. The corresponding transition temperature for an electron concentration of 5×10^{11} cm^{-2} was calculated as 6.0 K. This was apparently based on the assumption that the phonon modes to consider when determining the validity of the analytical calculations are those with energies close to kT. Using this criterion, it can be seen from Figs. 3.4 and 3.5 that the approximations for the screening factor and the overlap integral differ from the exact solution by only about 10% at a temperature of 3 K and an electron density of 5×10^{11} cm^{-2}, which would be quite good. However, the assumption that the dominant phonon modes are those with significant occupation numbers is not correct, and the approximations are considerably more inaccurate.

To solve Eq. (3.17) analytically, we must solve

$$F(T) \propto T^{n+1}\int_0^\infty (\frac{\hbar\omega_Q}{kT})^n \exp(-\frac{\hbar\omega_Q}{kT}) d(\frac{\hbar\omega_Q}{kT}), \tag{3.21}$$

where n is 6 for deformation potential scattering and 4 for piezoelectric scattering. This integrand has a maximum at $\hbar\omega_Q = nkT$, and is negligible for phonons with energies of only a few kT. When equipartition fails, scattering is dominated by phonon modes with energies much greater than kT. This is, of course, what we mean when we say that equipartition has failed badly, and it is a necessary condition for our approximation of the phonon occupation numbers by $N_Q = \exp(-\hbar\omega_Q/kT)$. However, the implications of

this for the analytic solutions of the transport equations have not been generally recognized. The analytic solution is accurate only at temperatures for which the approximations are valid for these high energy phonons. Based on this analysis of which phonon modes are dominant, the approximations for the overlap integral and the screening function at 3.0 K and an electron density of $5\times10^{11}/cm^2$ are an order of magnitude too large, a considerable difference from the 10% error suggested earlier. From Figs. 3.4 and 3.5 it can be seen that the approximations will be applicable only at extremely low temperatures and high electron concentrations.[59]

The failure of the analytic approximations destroys the effect of the Q dependence of the matrix element on the temperature dependence of the power loss. Thus, although the screened matrix element leads to a lower power loss than the unscreened matrix element, the temperature dependence of the power loss is not markedly changed by screening. It is therefore possible to directly test the importance of screening only at the extremely low temperatures for which the analytical approximations are valid.

The conclusion that high energy phonons are dominant was based on the solutions of the power loss equation with the approximations, but it is not materially changed without the approximations. Figure 3.6 shows the numerical calculation (without the approximations) of the power loss to deformation potential scattering at 1.0 K as a function of the phonon energy. The dominant phonons are those with energies of approximately 6kT. There is a secondary peak at an energy which corresponds to phonons with wave vectors $Q \cong 2k_f$, where k_f is the Fermi wave vector, and an abrupt decrease for larger wave vectors. Scattering is dominated by electrons near the Fermi energy, and the abrupt decrease in scattering occurs when the phonon wave vector exceeds the maximum

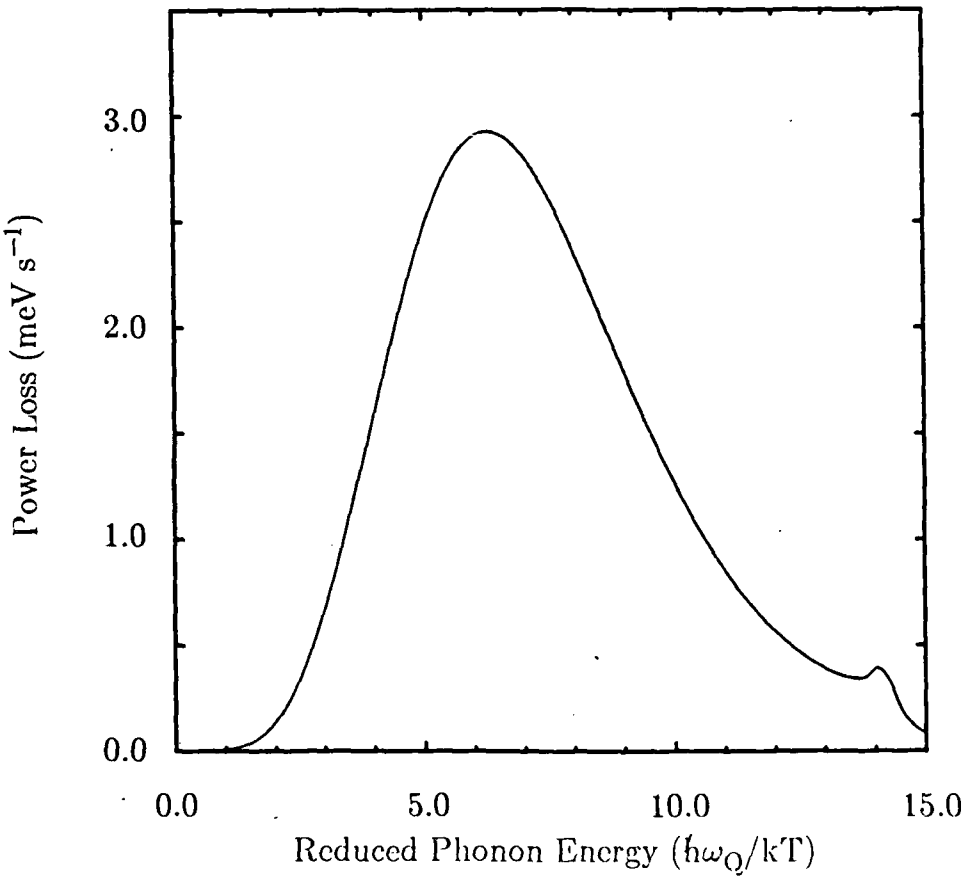

Fig. 3.6 The net power loss as a function of phonon energy for deformation potential scattering. Note that phonons with energies of only a few kT do not contribute substantially to the power loss. The secondary peak in this plot occurs at a phonon energy for which $Q \cong 2k_f$, corresponding to backward scattering of electrons at the Fermi energy. Calculated using a variational wave function for an electron concentration of 5×10^{11} cm^{-2}, a lattice temperature of 1.0 K, and an electron temperature of 1.05 K. Normalized for a deformation potential constant of 1.0 eV.

allowed by conservation of momentum. The limit is somewhat relaxed because the perpendicular component of momentum is not conserved.

At low temperatures, scattering falls off as the phonon occupation numbers decrease, and the dominant phonons are determined by the maximum of the factor $Q^n\exp(-\hbar\omega_Q/kT)$. At higher temperatures, scattering falls off when conservation of momentum limits the allowed scattering events to phonons with relatively small wave vectors, and the dominant phonons are those with wave vectors $2k_f$. Eventually, conservation of momentum limits the allowed scattering events to phonons with energies much less than kT, and equipartition becomes an accurate approximation. The crossover between the region where the maximum is determined by the factor of $Q^n\exp(-\hbar\omega_Q/kT)$ and the region where it is determined by conservation of momentum occurs gradually. Figure 3.7 is a graph of the power loss as a function of phonon energy at $T_l = 30$ K. The power loss is dominated by phonons with energies $\hbar\omega_Q \cong \frac{1}{2}kT$, and the error in using equipartition is about 30%. Equipartition does not become an accurate approximation until $2\hbar uk_f << kT$; for an electron density of 5×10^{11} cm^{-2} it is accurate to 10% or better when $T > 75$ K. This is considerably different from what we find in bulk semiconductors, which are not normally as degenerate as two dimensional electron gases, and for which equipartition is therefore accurate at lower temperatures.

Although equipartition does not become an accurate approximation until the temperature is relatively large, the power loss shows an approximately linear temperature dependence at much lower temperatures (above approximately 10 K for an electron concentration of 5×10^{11} cm^{-2}). This proportionality of the power loss to $T_e - T_l$ is what we expect when equipartition is accurate, but the proportionality constant calculated with

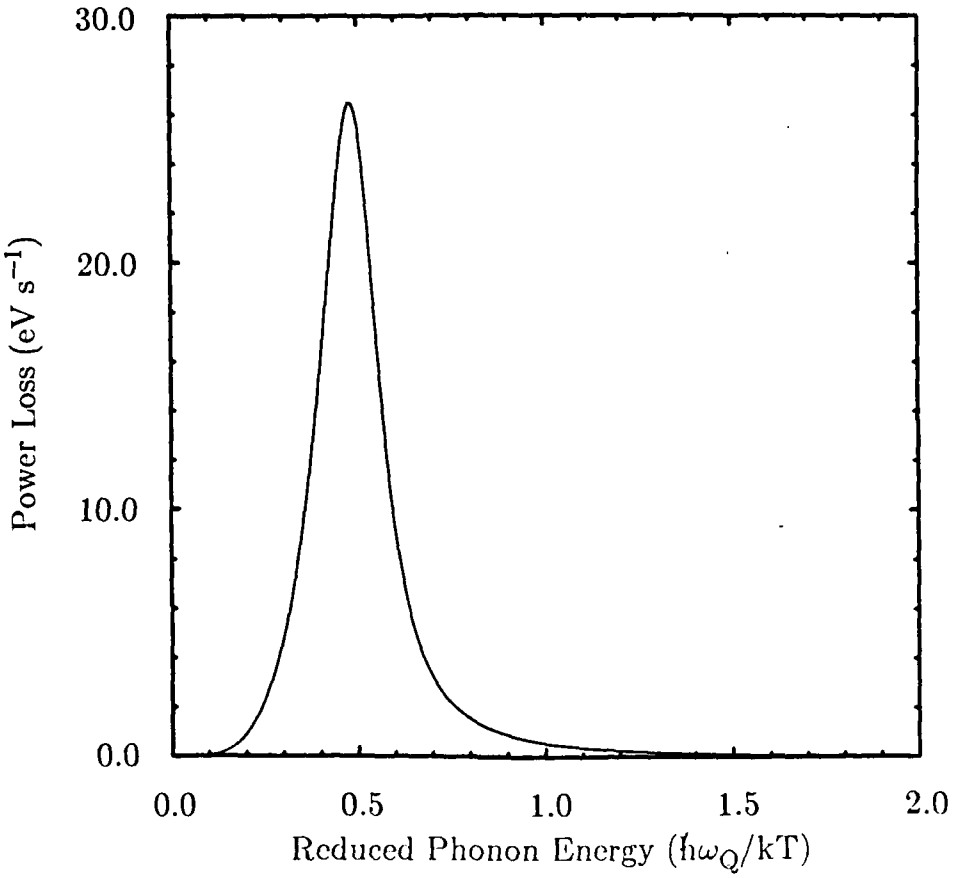

Fig. 3.7 The net power loss as a function of phonon energy at a lattice temperature of 30.0 K and an electron temperature of 30.05 K, temperatures for which equipartition is generally assumed to be accurate. The dominant scattering is by phonons with energies $\hbar\omega \cong$ ½kT, for which equipartition will produce a 30% error. Calculated for a two-dimensional electron gas density of 5×10^{11} cm^{-3} using a variational wave function. For this electron density equipartition does not become accurate to 10% until the temperature exceeds 75 K.

the assumption of equipartition will be wrong. Thus the experimental observation of a power loss (or mobility) proportional to temperature does not necessarily indicate that equipartition is a valid approximation.

At relatively low electron concentrations, the approximations may fail even at extremely low lattice temperatures. A recent study has reported measured power loss rates of electrons in a $Al_xGa_{1-x}As/GaAs$ superlattice at temperatures ranging from 100 mK to 385 mK.[60] The electron concentration was 1.7×10^{11} cm^{-2}. It was assumed that deformation potential scattering was negligible and that the analytic approximations were applicable, which would lead to a power loss rate with a T^5 dependence. However, to fit the experimental data to this model it was necessary to use five adjustable parameters. For the range of data in this study the more exact numerical solution shows that we would expect this model to give a temperature dependence between $T^{3.8}$ and $T^{4.4}$, depending on the lattice temperature and the value used for the deformation potential. We emphasize that this temperature dependence has no direct physical meaning, but is merely the result of fitting a model to the data. With a different range of data the results would be different. Note that the energy loss to deformation potential scattering would be important if the larger values of the deformation potential were used. The failure of the analytic approximations partially explains the discrepancy between the energy relaxation rate determined in this experiment and the rate which was expected from the analytic theory.

4. EXPERIMENTAL TECHNIQUES AND CONSIDERATIONS

4.1. Measuring the Power Loss and the Electron Temperature

In the preceding chapter we derived the equations that relate $<d\epsilon/dt>$ to Z, T_e, T_l, ϵ_f, and the wave function $\phi(z)$ of the electron. In this chapter we discuss the experimental measurements with which we will compare the theory.

Experimentally, it is convenient to measure the relationship between $<d\epsilon/dt>$ and T_e for fixed values of T_l, ϵ_f, and the electron wave function. We then calculate the expected power loss and adjust the deformation potential constant Z to give the best agreement between the theory and the experimental data.

The average power loss is easily measured. In the steady state, the total power lost by the conduction electrons to the lattice is exactly balanced by the input power from the electric field. The input power is simply the Joule heating, given by I^2R, where I is the input current and R is the resistance. We infer the average power loss per electron by dividing the input power by the measured electron concentration and sample area. The electron temperature is more difficult to measure.

A number of techniques have been developed to measure the electron temperature, some more accurate than others. What is required is a measurable parameter which is a function of the electron temperature. There must be some method of calibrating its dependence on the electron temperature, and it must be independent of any other parameters which are varied, either during the calibration or during the measurement of the relationship between T_e and $<d\epsilon/dt>$.

One common technique used to measure the electron temperature depends on the variation of the mobility[35] with temperature. This method has the advantage of simplicity. First the temperature dependence of the mobility is calibrated by measuring the low field mobility at various lattice temperatures. The input power used during the calibration must be small enough that the electron temperature can be assumed to be equal to the lattice temperature. The lattice temperature is then fixed, and the input power increased. At large input powers the electron temperature is raised above the lattice temperature, and the electron temperature is inferred by comparing the mobility at large input powers with the calibration curve.

Although this method offers the advantage of simplicity, it is of questionable accuracy. The problem arises because of the difficulty in separating the T_e dependence of the mobility from the T_l dependence. The mobility may be directly affected by the lattice temperature as well as the electron temperature because of the dependence of phonon scattering on the lattice temperature. Thus the calibration curve will in most cases reflect the effects of both T_l and T_e, in which case it cannot be used to determine T_e.

A similar method infers T_e from the temperature dependence of the sample resistance, but includes an additional uncertainty due to the T_l dependence of the carrier concentration. This method has been used in previously reported measurements of the power loss in an $Al_xGa_{1-x}As/GaAs$ superlattice.[60] As discussed in Chapter 3, the measured power loss did not have the functional form predicted by a precise numerical calculation of the theoretical power loss, and the measured power loss was two orders of magnitude larger than expected. It was suggested[60] that this anomalous power loss can be explained if the electron distribution function deviates from the Fermi-Dirac function

used in the theoretical analysis. Another possibility is that the measurement of the electron temperature was inaccurate. Because the power loss depends on the temperature raised to a large power, a small error in T_e leads to a large error in the calculated power loss. An alternative method of measuring T_e is necessary.

4.2. The Shubnikov–de Haas Oscillations

In this work we use the strong temperature dependence of the Shubnikov–de Haas (SdH) oscillations, which are oscillations in the resistance of a sample that occur when an applied magnetic field is ramped up or down.[61] The amplitude of the SdH oscillations is strongly dependent on the electron temperature, and thus provides a sensitive thermometer.

The SdH oscillations occur because of the effect of a magnetic field on the density of states available to the electrons. In a two–dimensional system with no applied magnetic field, the electrons have two degrees of freedom and the density of states is a constant, $D(\epsilon) = m^*/\pi\hbar$. When a magnetic field is applied perpendicular to the plane of the two–dimensional system the electrons lose both degrees of freedom. They must follow circular orbits around the magnetic field lines. The Hamiltonian for this system was first solved by Landau,[62] and these orbits are called Landau levels. The energies of the Landau levels are given by $E_n = (n + \frac{1}{2})\hbar\omega_c$, where n is a quantum number and ω_c is the cyclotron frequency, $\omega_c = eB/m^*$. The allowed energies are now at discrete points separated by $\hbar\omega_c$, and the density of states is no longer a constant. The idealized density of states for a two–dimensional system in a magnetic field consists of a series of delta functions at the energies of the Landau levels, as shown in Fig. 4.1a). In actual systems the electrons are scattered by impurities, phonons, and other imperfections, and this

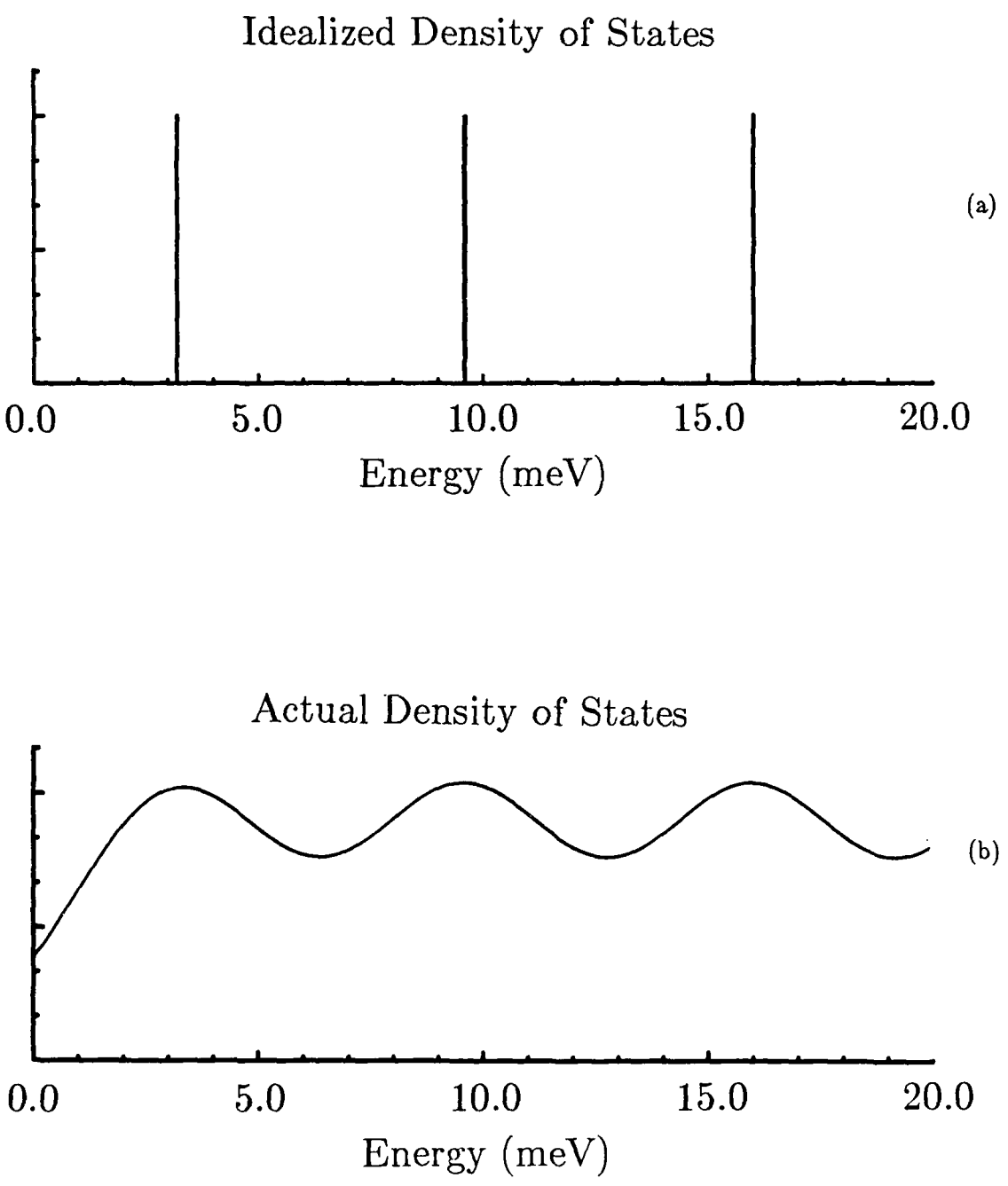

Fig. 4.1 a) The density of states of a two-dimensional electron gas in a magnetic field as a function of energy without the effects of scattering. b) The density of states with the effects of scattering included. Calculated for a Dingle temperature of 17 K and a magnetic field of 37 kG, the approximate conditions of our experiment.

scattering of the electrons results in broadening of the delta functions, as shown in Fig. 4.1b). The broadening may be regarded somewhat imprecisely as arising from the Heisenberg uncertainty principle, $\Delta E\tau \cong \hbar$, where ΔE is a measure of the broadening and τ is a scattering time.

This change in the density of states can have a dramatic effect on the average scattering rate and hence on the resistance. The scattering rate for a given electron is proportional to the density of final states available to the electron, and the total resistance depends on the average of the scattering rate over all occupied states. In a degenerate system the Pauli exclusion principle prevents electrons with energies many kT_e below the Fermi energy from scattering, and the resistance is determined by the scattering of electrons near the Fermi energy.

If a magnetic field applied perpendicular to a degenerate two–dimensional electron gas is ramped up or down, then the energies of the Landau levels change, and the peaks in the density of states move through the Fermi energy. The change in the density of states at the Fermi energy changes the overall scattering rate, and the resistance of the sample oscillates as successive Landau levels move through the Fermi energy. Figure 4.2 shows an example of the SdH oscillations in one of our samples.

There are a number of conditions which must be met if the SdH oscillations are to be observed. If the broadening of the Landau levels due to scattering exceeds the separation between levels, then there will not be any significant energy dependence of the density of states. From the Heisenberg uncertainty principle we see that the broadening of the Landau levels will be less than the separation between levels when $\omega_c\tau > 1$ or equivalently when $\mu B > 1$, where we use the standard expressions to relate ω_c to μ.

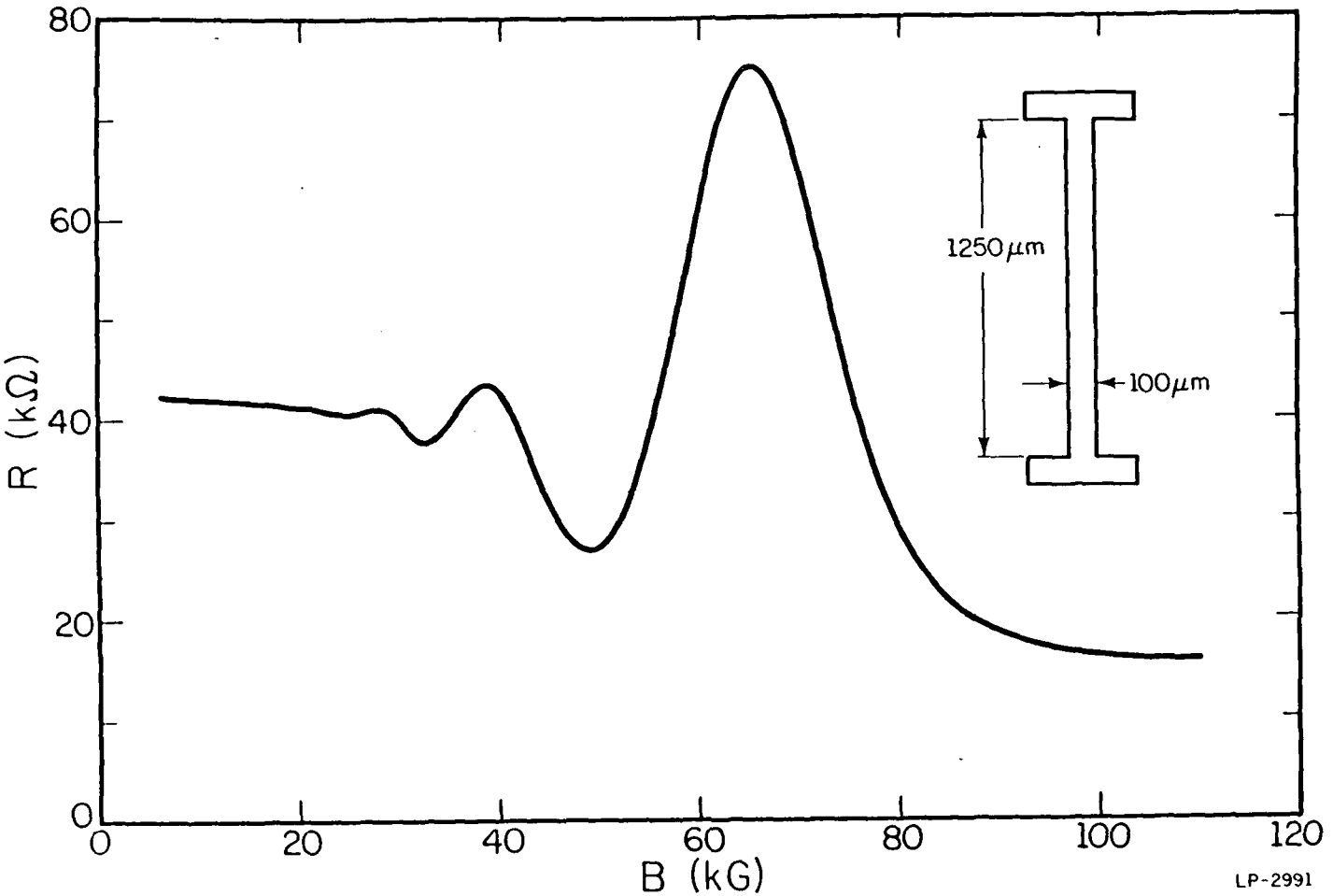

Fig. 1.2 The Shubnikov-de Haas oscillations in one of our samples. The lattice temperature was 4.2 K and the electric field was 50 mV cm^{-1}, which is small enough that $T_e \cong T_l$. The inset shows the device geometry used for these measurements.

Physically, this means that the average electron makes at least one orbit before scattering. It is apparent that relatively large magnetic fields are necessary to observe the SdH effect. The curve shown in Fig. 4.2 was made using a sample with a mobility $\mu \cong 20\,000\ \mathrm{cm^2\ V^{-1}\ s^{-1}}$, for which the effect should start at a magnetic field of approximately 5 kG. It can be seen that multiple periods of a convenient amplitude appear only at considerably larger magnetic fields.

The condition $\mu B > 1$ assures that the density of states varies with energy. It is also necessary that the averaging of the scattering rate over energies near the Fermi energy include significant contributions from only a small range of the density of states, or the variation will be averaged out. This condition is met when $kT_e < \hbar\omega_c$, which limits the significant contributions to a single period of the oscillations in the density of states. For typical magnetic fields the SdH effect is observed only at temperatures below approximately 15 K.

Finally, it is necessary that the sample be degenerate if the Landau levels are to move through the Fermi energy. If we are to see oscillations then we require that $\epsilon_f \gtrsim \hbar\omega_c$ at the magnetic field for which $\mu B > 1$. Thus the sample must be strongly degenerate. In some samples it is not possible to satisfy $\mu B > 1$ and $\epsilon_f \gtrsim \hbar\omega_c$ simultaneously, and the SdH oscillations are not observed. This is why this method of measuring the deformation potential constant cannot be applied to bulk GaAs.

The theory of the SdH oscillations depends on quantum solutions of the equations of motion and on the details of the scattering events that broaden the Landau levels, and is therefore quite complicated. With some approximations appropriate to the conditions of our experiment, the theory predicts that the change in resistance is given by

$$\Delta R \propto R_0 \frac{CkT_e/\hbar\omega_c}{\sinh(CkT_e/\hbar\omega_c)} \exp(-CkT_D/\hbar\omega_c) \cos(\frac{2\pi\epsilon_f}{\hbar\omega_c} - \frac{\pi}{4}) \tag{4.1}$$

where R_0 is the resistance in the absence of a magnetic field, C is a constant, and T_D is a measure of the Landau level broadening called the Dingle temperature.[61] Note that the amplitude of the oscillations is exponentially damped by the Landau level broadening, and that the amplitude increases with increasing magnetic field. There are a number of additional predictions of the theory.

The resistance oscillates as successive Landau levels pass through the Fermi level, and the period of the oscillations is determined by the Fermi energy. From Eq. (4.1) we can see that the period is given by

$$\Delta(\frac{1}{B}) = \frac{\hbar e}{m^*} \frac{1}{\epsilon_f} = \frac{e}{\pi\hbar} \frac{1}{n} \tag{4.2}$$

where $\Delta(1/B)$ is the change in the inverse magnetic field between peaks in the resistance, n is the sheet carrier concentration, and the remaining symbols have their usual meanings. This equation may also be derived using simple semiclassical arguments which depend only on the general form of the density of states in a magnetic field, and not on the details of the scattering or the Landau level broadening. Because of its generality, it has proven quite accurate, and it is commonly used to determine the carrier concentration in $Al_xGa_{1-x}As/GaAs$ systems at low temperatures. We use the SdH oscillations to measure the carrier concentration, which we must know in order to infer the power loss per electron from the total input power.

The theory also predicts that there is a strong electron temperature dependence of the amplitude of the SdH oscillations, and this is our primary interest. The amplitude of the oscillations depends on the variation in the average scattering rate, and the averaging

of the scattering rate depends on kT_e through the electron distribution function. If kT_e is large, then the averaging smooths out the variation in the density of states, and the oscillations will be of small amplitude. Conversely, if kT_e is small, then the oscillations will have large amplitudes. Figure 4.3 shows the SdH oscillations in one of our samples at a temperature of 2.7 K, and Fig. 4.4 shows the SdH oscillations in the same sample at a temperature of 8.86 K. Note the large difference in the amplitude of the oscillations. Because the temperature has a strong effect on the amplitude of the oscillations the amplitude is a quite sensitive measure of the electron temperature.

In principle, Eq. (4.1) can be used to exactly predict the temperature dependence of the amplitude of the the oscillations. In practice, the amplitude depends on too many unknown parameters for the theory to be accurate enough for our purpose, and we must calibrate the temperature dependence experimentally. This is done by measuring the amplitude of the oscillations at a sequence of lattice temperatures using an input power small enough that the electron temperature is the same as the lattice temperature. The calibration will be accurate as long as the amplitude does not depend directly on T_l.

The amplitude will depend on T_l only if the Landau level broadening depends on T_l, and this broadening is determined by the scattering mechanisms. In high mobility (over approximately 2×10^5 cm^2 V^{-1} s^{-1}) modulation doped samples, lattice scattering is a significant part of the total scattering, and the variation in the density of states will then depend on the lattice temperature. In order to avoid this problem we have used relatively low mobility samples ($\approx$20 000 cm^2 V^{-1} s^{-1}) in which impurity scattering is dominant. Impurity scattering depends on the electron energy (and therefore on the electron temperature) but not on the lattice temperature. Hence the density of states may show

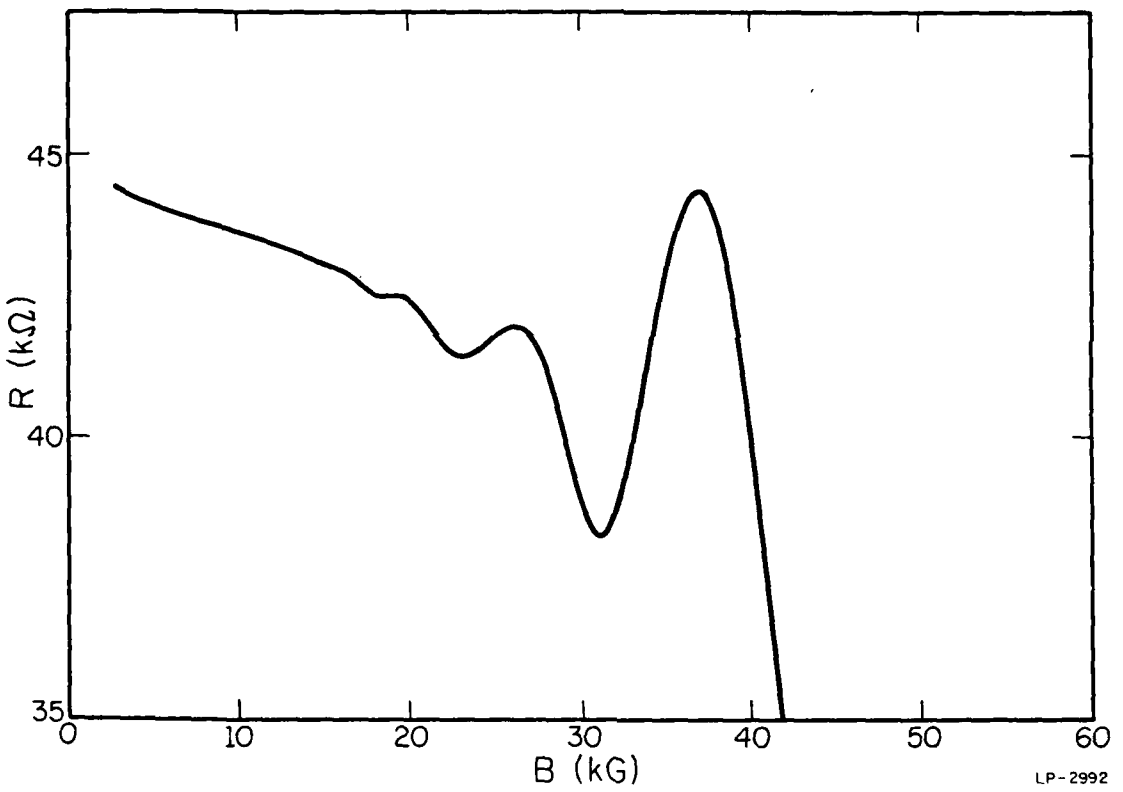

Fig. 4.3 Detail of the calibration of the amplitude of the Shubnikov–de Haas oscillations. The lattice temperature was 2.70 K. The electron concentration, as determined from the period of the oscillations, was 4.7×10^{11} cm^{-2}.

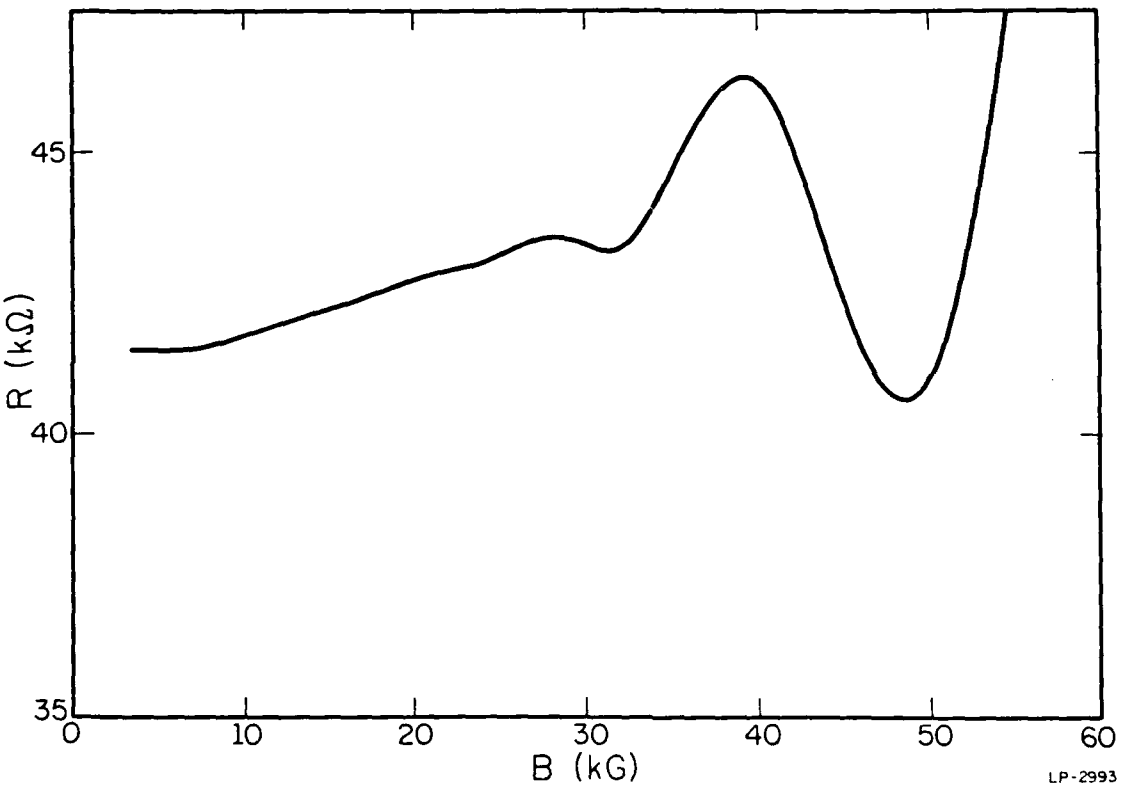

Fig. 4.4 The Shubnikov–de Haas oscillations in the same sample as in Fig. 4.3 at a lattice temperature of 8.86 K. Note the decreased amplitude of the oscillations in comparison with those shown in Fig. 4.3. Note also that the nonoscillatory component of the magnetoresistance has changed.

some temperature dependence, but it will depend only on the electron temperature, and the calibration will be accurate.

This method of measuring T_e depends on the changes in the scattering rate that occur as the density of states changes. However, we compare our experimental data to calculations of the power loss in which we have assumed that the density of states is constant. In order to minimize the discrepancy between the conditions of the experiment and the theory we measure the amplitude of the SdH oscillations at a magnetic field for which the amplitude of the oscillations is small (less than 15% of the zero field resistance.) Because the resistance has deviated only slightly from the zero field value we can be sure that the power loss has deviated only slightly also.

4.3. Other Contributions to the Magnetoresistance

In addition to the SdH oscillations, there are a number of other components to the magnetoresistance. One of them depends on the geometry of the sample.[63] The geometrical contribution is maximized in short, fat samples (the Corbino geometry) and minimized in long, narrow samples. Under the conditions of our experiment the Corbino geometry gives a geometrical magnetoresistance $\Delta R/R_0 \cong \mu^2 B^2$, which dominates all other components. Our initial experiments were done with devices that had a 1:1 length–to–width ratio and a moderate contribution from the geometrical effect. Later experiments, from which the data in this thesis was taken, used devices with a 12½:1 ratio, as shown in the inset of Fig. 4.1. This ratio is large enough to essentially eliminate the geometrical contribution to the magnetoresistance. The source–drain spacing of these devices was 1250 μm, which is large enough to achieve small electric fields with con-

veniently measured source–drain voltages. Small electric fields are necessary during the calibration phase to eliminate any significant heating of the electrons.

There are other components of the magnetoresistance which cannot be eliminated as the geometrical component can. The localization correction depends on random fluctuations in the potential that an electron sees, and leads to a negative magnetoresistance[64]. The electron–electron interaction between diffusively moving electrons can lead to either a positive or a negative magnetoresistance.[65]. The interaction magnetoresistance has not been studied extensively, and is not well understood. We expect the magnetoresistance in each case to depend on T_e, but this has not been conclusively demonstrated experimentally.

4.4. The Sample Structure

The basic structure used in our experiment is a modulation doped single heterostructure. A diagram of the structure which was used for most of the data we present is shown in Fig. 4.5. In principle it is possible to calculate the doping levels and layer thicknesses necessary to produce a sample with the desired properties. In practice, there is too much uncertainty in the ionization energy of donors in the $Al_xGa_{1-x}As$ and in the calibration of the doping levels reached during the crystal growth process for the calculated parameters to provide anything other than general guidelines, and it is necessary to adjust the parameters empirically.

The criterion for choosing the parameters is that they should provide a two–dimensional electron gas in the GaAs with no parallel conduction through the $Al_xGa_{1-x}As$. It is necessary that the nominally undoped GaAs layer in which the

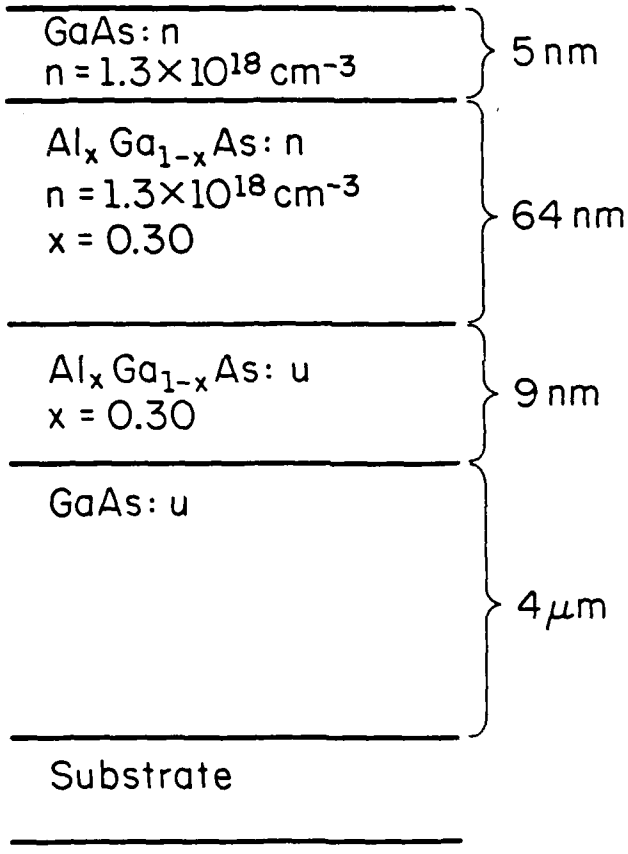

Fig. 4.5 The sample structure used in our experiments. Slight variations on this structure were also tried, as discussed in the text.

two–dimensional electron gas is to form be slightly P type. At the temperatures of our experiment the effective density of states in the conduction band is of the order of 10^{15} cm^{-3}. If the bulk material is even slightly N type then it will be degenerate, and there will be no band bending to confine the electrons at the interface.

Samples in which the GaAs is N type do not provide strong confinement of the electrons at the interface, and the electrons are effectively three–dimensional. Although these samples may be degenerate, the Fermi level is much closer to the conduction band then it would be if the electrons were concentrated near the interface. The mobility is much lower because of the decrease in screening which accompanies the lowering of the Fermi level and because of the increased impurity scattering. As a result it is not possible to satisfy $\mu B > 1$ and $\epsilon_f \gtrsim \hbar\omega_c$ at the same time, and the SdH effect is not observed. However, the resistivity remains low, indicating that a considerable number of carriers are present. These samples were not suitable for our measurements.

In the samples which we use for our measurements of the deformation potential constant we have verified that the conductivity is through a two–dimensional electron gas by observing the disappearance of the SdH oscillations when the sample is tilted so that the magnetic field is parallel to the heterointerface. When the sample is oriented in this way there are no SdH oscillations because the confinement of the two–dimensional electrons prevents them from describing Landau orbits, and there is hence no variation in the density of states.

A second potential problem occurs if the doping level in the $Al_xGa_{1-x}As$ is too large, which prevents it from fully depleting. The parallel conduction path through the $Al_xGa_{1-x}As$ prevents an accurate measurement of the input power to the two dimen-

sional electron gas, and would lead to errors in our measurement of the deformation potential constant. The onset of parallel conduction has been studied extensively. It has been noted that parallel conduction contributes a large positive nonoscillatory component to the magnetoresistance.[66] Figure 4.6 shows an example of the magnetoresistance in a sample with parallel conduction through the $Al_xGa_{1-x}As$. We did not use samples which exhibited this large nonoscillatory magnetoresistance for our measurement of the deformation potential constant.

4.5. Experimental Equipment

Because of the high magnetic fields necessary to observe the SdH oscillations we use a superconducting magnet. The magnet, made by Intermagnetics General Corporation (IGC), provides a maximum field of up to 130 kG in a bore of 3.8 cm, and may be ramped to full strength in about 15 minutes. The magnetic field strength is measured using a calibrated probe provided by IGC. The probe consists of a coil of copper wire with a magnetic field-dependent resistance, and has been calibrated by IGC to better than 1%. The signal from the probe is linearized and is used to drive one axis of an XY plotter on which we record the SdH oscillations.

To calibrate the temperature dependence of the oscillations we must be able to vary the lattice temperature. The superconducting magnet has been designed to accept the Janis Super Varitemp insert to allow variable temperature measurements. This insert provides a sample chamber which is insulated from the main magnet chamber, and a small leak valve to admit liquid helium from the magnet chamber into the sample chamber. The temperature is maintained at 4.2 K by filling the sample chamber with liquid He. Temperatures below 4.2 K are obtained by using a roughing pump to draw a

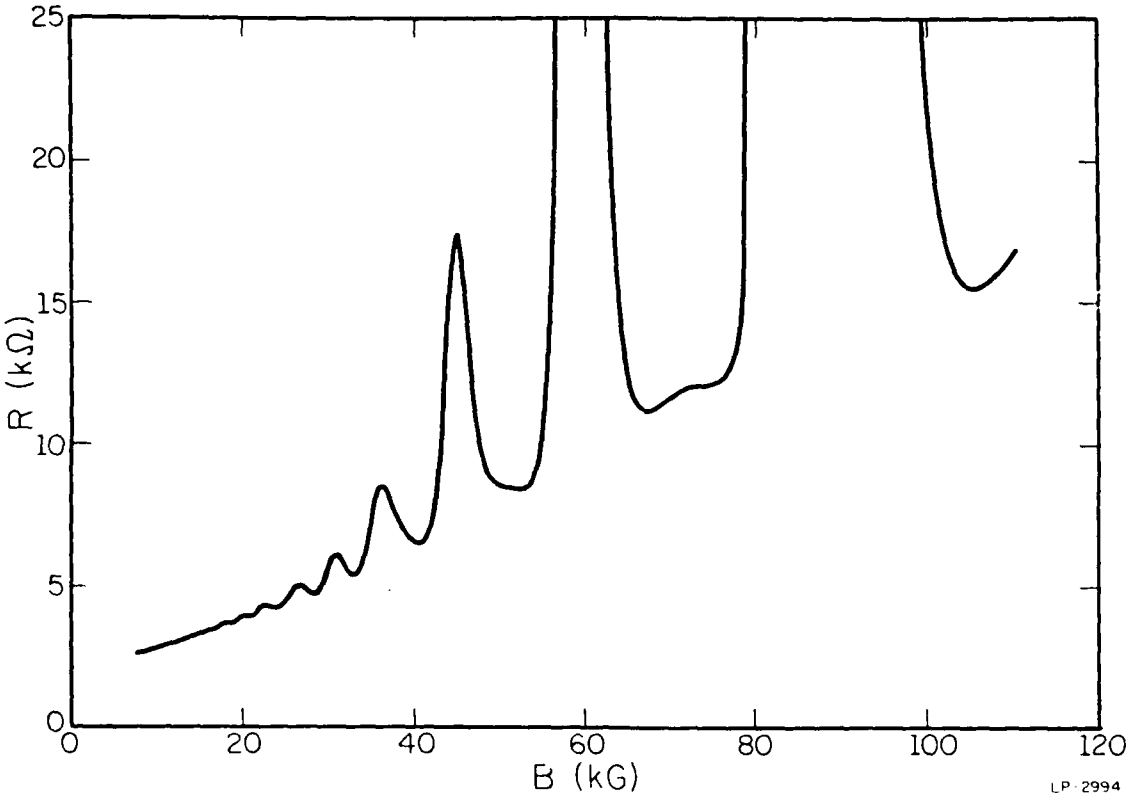

Fig. 4.6 The Shubnikov–de Haas oscillations in a sample with parallel conduction through the $Al_xGa_{1-x}As$. The concentration in this sample is 9.7×10^{11} cm^{-2}, considerably higher than in the previous figures. This sample used a thicker $Al_xGa_{1-x}As$ layer which increased the electron concentration, but was too thick to completely deplete, resulting in parallel conduction. Despite the low electric field there is a large positive nonoscillatory component of the magnetoresistance. The lattice temperature was 4.2 K. The double valleys that appear at high magnetic fields are the result of spin splitting of the Landau levels.

partial vacuum on the sample chamber. A Lake Shore Cryogenics 329 vacuum regulator connects the roughing pump to the sample chamber and maintains a constant pressure. The regulator is easily adjusted and stable enough to maintain the temperature constant to within a few mK. The lowest temperature that we can achieve with this system is approximately 1.5 K, although at temperatures below 2.17 K (the λ point of ^{4}He) the temperature is somewhat unstable. At temperatures below 4.2 K the sample is in constant contact with liquid He, which provides good temperature stability and a large thermal mass to absorb any input power.

The Super Varitemp is also designed to provide temperatures above 4.2 K. In this mode the leak valve is opened only enough to slowly admit liquid He to the sample chamber. Power is applied to a resistive heater at the bottom of the sample chamber, and the liquid He is vaporized as it is admitted. The He vapor escapes out a vent and cools the sample as it passes over it. This does not provide as high a degree of temperature stability as is available with the sample in contact with liquid He, but with care the temperature drift can be reduced to less than 0.05 K over the time necessary to complete the magnetoresistance measurement, which is adequate for our experiment.

The lattice temperature of the sample is measured using a Lake Shore Cryogenics carbon–glass resistance thermometer which is attached directly to the sample holder. A carbon–glass thermometer is used because it is relatively insensitive to the magnetic field, showing only a few percent change in resistance as the magnetic field is increased to full strength. The more commonly used GaAs or Si temperature sensing diodes would show a few hundred percent change under similar conditions, and are therefore unsuitable.

The sample resistance is measured by injecting a current and measuring the resulting voltage. Some studies have found that at very high electric fields it is necessary to make pulsed measurements in order to avoid heating of the crystal lattice (hot phonon effects.) Using the known heat capacities and thermal diffusivity of GaAs, we can calculate that the maximum input power used in our experiment (approximately 3 mW cm^{-2}) can produce a temperature rise of much less than 1 mK, and we conclude that pulsed experiments are therefore not necessary at the electric field strengths of our experiment.

We use a Keithly 225 constant current source to make the dc measurements. The sample resistance is approximately 40 kΩ, and the maximum field we apply is 10 V cm^{-1}. The sample resistance is much larger than either the resistance of the leads or the resistance of the contacts, and it is not necessary to make a four–wire measurement of the resistance.

The voltage induced across the sample is not large enough to drive the XY plotter directly and must be amplified first. We use a PAR 113 differential amplifier for this. The high–frequency rolloff is set at 10 Hz to reduce the noise, and the low–frequency rolloff is set at dc. The system is calibrated by substituting precision resistors in place of the sample and adjusting the amplifier gain and offset as necessary. For very low induced voltages it is necessary to account for the thermal EMFs that may be generated in the wires that connect the amplifier (at 300 K) to the sample (at 4.2 K.) We can reduce these EMFs by using identical wires for the source and drain connections so that the EMF in the wires will cancel out. In practice there remains an EMF of around 1 mV, apparently due to inhomogeneities in the wires.

4.6. Calibrating the T_e Dependence of the SdH Oscillations

The first step in measuring the electron temperature is to calibrate the temperature dependence of the amplitude of the SdH oscillations. As we have previously discussed, this is done by measuring the amplitude at a sequence of lattice temperatures while using a low enough input power that we may accurately approximate $T_e = T_l$. After experimentally determining the dependence of T_e on the input power we have calculated the expected temperature increase for the input power used during the calibration and found it to be less than 1 mK, which confirms the accuracy of the approximation that $T_e = T_l$. The most difficult part of the calibration is the measurement of the amplitude of the oscillations.

The measurement of the amplitude of the SdH oscillations is complicated by the nonoscillatory magnetoresistance that is present in all samples. This nonoscillatory component can be seen clearly in Figs. 4.2, 4.3, and 4.4. The measurement of the amplitude of the oscillations must either include this component or account for it. We have measured the amplitude of the SdH oscillations in two different ways.

One approach is to estimate the nonoscillatory component of the magnetoresistance and to subtract it out of the measured amplitude. This approach has the advantage that it does not directly include the nonoscillatory component, which is not as well understood as the SdH oscillations are. It has the disadvantage of the uncertainty in the estimate of the nonoscillatory component. The other approach is to measure the total magnetoresistance, including both the SdH oscillations and the nonoscillatory component of the magnetoresistance. This approach has the advantage that it is simple and does not require an *ad hoc* estimate of the nonoscillatory component. Furthermore, since the

nonoscillatory component is often a small part of the total magnetoresistance, and since we observe experimentally that the nonoscillatory component depends at least partially on the electron temperature, this approach introduces at most a small error. Because of the importance of this measurement to our experiment we have tried both approaches.

Theoretically, the most justifiable simple estimate of the nonoscillatory magnetoresistance is quadratic in the magnetic field.[64,65] We first attempted to include the nonoscillatory component by using a computer to do a least–squares fit of the magnetoresistance to a theory which included both the SdH oscillations and a quadratic nonoscillatory component. It was found that this did not produce consistent results, probably because of the large number of adjustable parameters necessary. For our data analysis we therefore adopted the much simpler assumption that the nonoscillatory component was linear in the magnetic field. This is certainly not accurate, but it may be accurate enough for the limited region of the magnetic field that we are interested in, and most importantly, it allows for a more consistent estimate of the nonoscillatory component. The amplitude of the oscillation is then measured from the baseline which is our estimate of the nonoscillatory component. This method leads to considerable scatter in the data points, apparently because the nonlinearities in the magnetoresistance prevent us from accurately accounting for the nonoscillatory component. Consequently, for most of our data analysis we have instead measured the amplitude of the oscillations including the nonoscillatory component of the magnetoresistance.

In this case we measure the amplitude of the peak at 37 kG using the valley at 32 kG as our reference point. This measure therefore includes the SdH amplitude at 32 kG,

the SdH amplitude at 37 kG, and the change in the nonoscillatory component between these two fields. This has the advantage of eliminating the uncertainty in our estimates of the nonoscillatory component, and eliminating the scatter in the data points. Figure 4.7 shows a calibration curve made using this method.

This measurement is accurate only if the nonoscillatory component of the magnetoresistance depends on the electron temperature, or if it is a small enough contribution as to be negligible. Our results verify the accuracy of this measurement. Figure 4.8 shows two magnetoresistance curves. One is a calibration curve, made with 200 nA of excitation current at a temperature of 7.38 K. The second curve was made at a lattice temperature of 3.40 K and an excitation current of 9.75 μA. From the calibration curve we see that the electrons are heated to an approximate temperature of 7.40 K. In Fig. 4.8 the two curves are offset slightly so as to illustrate the differences, which are minimal. The only significant difference is the deviation of the curves at the minimum of resistance which occurs at 48 kG. This deviation is easily understood. The calibration curve is for a constant electron temperature, $T_e = 7.38$ K. The other curve was made at a constant current. Because the sample resistance varied, the input power varied, and the electron temperature is not constant. The reduced resistance in the valley at 48 kG reduced the input power, and therefore lowered the electron temperature, leading to a larger amplitude oscillation. The deviation of the electron temperature from a constant is substantial only for large amplitude oscillations, which we do not use in our measurement of the electron temperature.

Both calibration curves lead to essentially the same results, although there is consid-

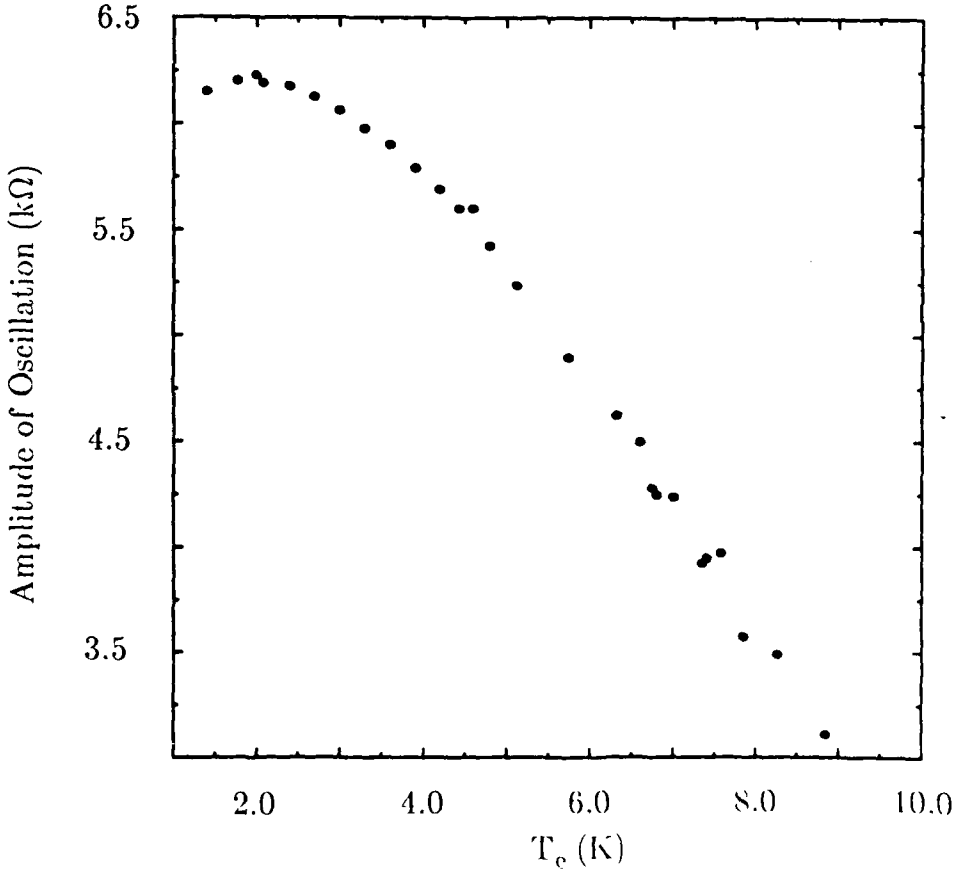

Fig. 4.7 A calibration curve showing the amplitude of the oscillations versus T_e.

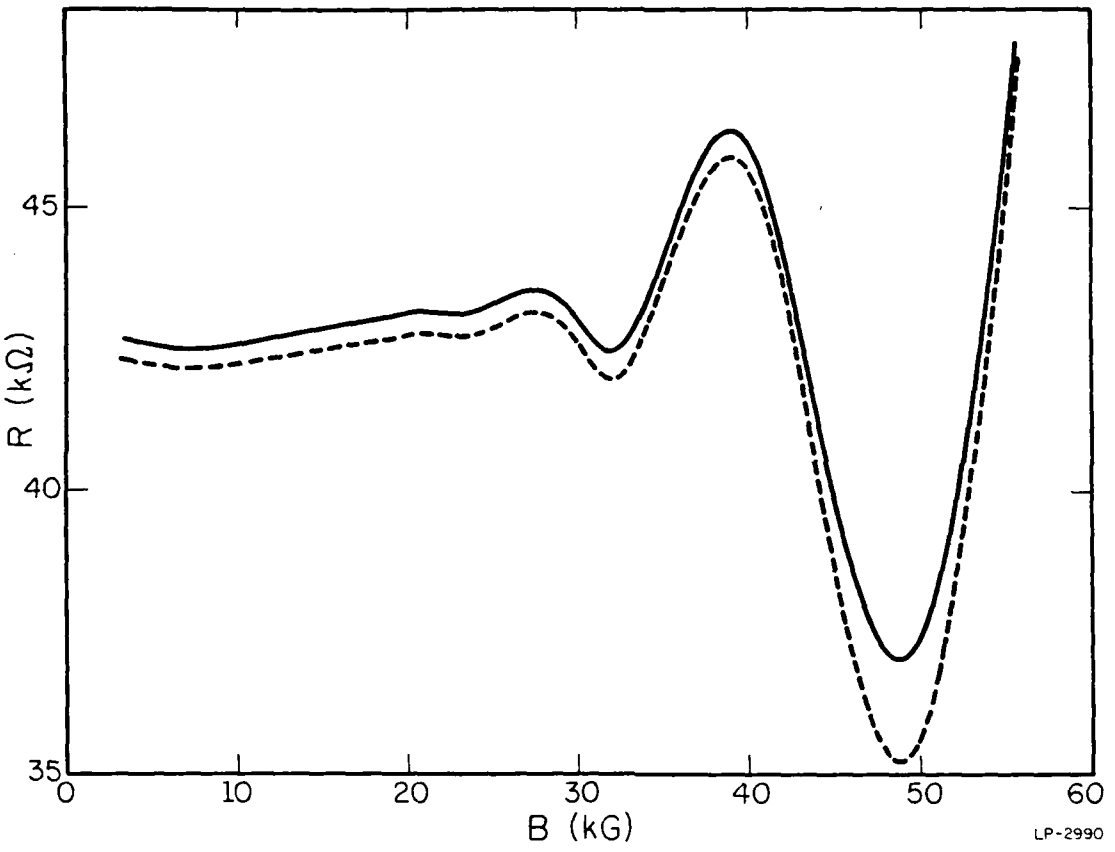

Fig. 4.8 A comparison of a calibration curve, made at $T_1 = 7.38$ K and an input current of 200 nA, with a curve from the same sample made at $T_1 = 3.40$ K and an input current of 9.25 μA, for which the electron temperature is predicted to be approximately 7.40 K. The curves have been offset slightly for easier comparison. Note how closely they match. The discrepancy between the curves at 48 kG is explained in the text.

erably more scatter in the data points when we attempt to eliminate the contributions from the nonoscillatory component of the magnetoresistance. All of the data which we present in Chap. 5 was derived from calibration curves in which we included the nonoscillatory component.

5. EXPERIMENTAL DATA AND ANALYSIS

5.1. Experimental Results

We have used the calibration curves discussed in Chap. 4 to measure the electron temperature as a function of the input power at various lattice temperatures.[67] The input power is converted to a power loss per electron by dividing by the electron concentration and the area of the sample, as discussed previously. Figure 5.1 shows experimental data from one device and the theoretical calculation of the power loss. The deformation potential constant was adjusted to give the best agreement between the experimental data and the theoretical calculations, where the best fit is the one which minimizes the sum of the square errors. Table 5.1 lists the values of the parameters used in our calculations. The scatter in the data points taken at a lattice temperature of 5.5 K is due to the difficulty in stabilizing the temperature of the sample chamber at temperatures above 4.2 K.

The theoretical power losses shown in Fig. 5.1 were calculated for a deformation potential constant of 15.8 eV, which produced the best simultaneous fit of the data at all lattice temperatures. This calculation included the self–consistent wave function and the effects of screening. We have also determined the deformation potential constant which best explains the data at each lattice temperature independently. This required deformation potential constants of 15.5 eV at 2.4 K, 15.9 eV at 4.2 K, and 16.0 eV at 5.5 K. The differences in the value of the the deformation potential constant deduced at different lattice temperatures reflect only a 6% change in the acoustic phonon scattering rate, and are not significant.

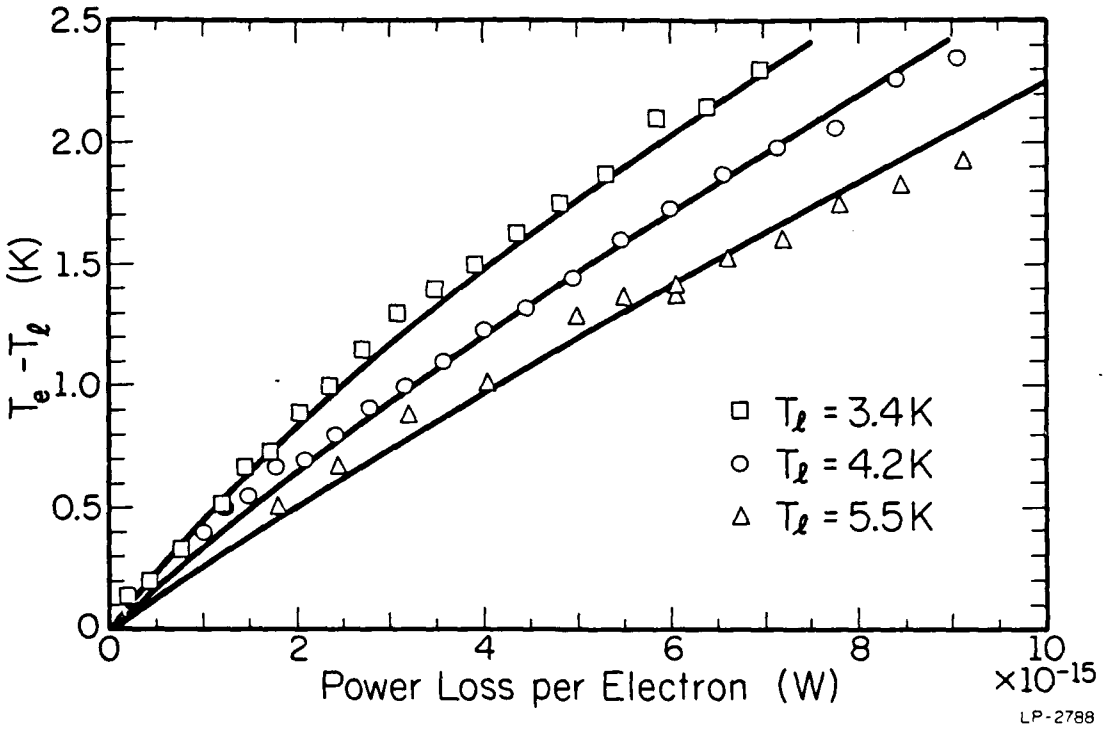

Fig. 5.1 The experimental data from one sample and the theoretical power losses for a deformation potential of 15.8 eV. The scatter in the data points at a lattice temperature of 5.5 K is caused by instabilities in the temperature of the sample chamber.

Table 5.1

Parameters Used in Calculations

Effective Mass	m^*/m_0	0.067
Longitudinal Sound Velocity	u_l	5.24×10^5 cm s^{-1}
Transverse Sound Velocity	u_t	2.99×10^5 cm s^{-1}
Piezoelectric Constant	eh_{14}	1.45×10^7
Static Dielectric Constant	ϵ_r	12.9
Density	ρ	5.36 g cm^{-3}

Data taken from other devices required a change of up to 1 eV in the deformation potential constant necessary to fit the data. This corresponds to about a 10% change in the power loss, and is within the expected experimental error. Devices which were cycled repeatedly between room temperature and liquid He temperatures exhibited increased power loss for a given electron temperature and required larger values of the deformation potential constant to model the data. This cannot, of course, reflect any real change in the deformation potential constant. It is probably the result of damage to the interface caused by repeated cycling of materials with different thermal constants. The data presented in Figs. 5.1 and 5.2 was taken from a device which was cooled to liquid He temperatures only once.

In addition to the data shown in Fig. 5.1 we have also measured the power loss at a lattice temperature of 1.57 K. The data taken at 1.57 K is best fit using a deformation potential of 16.8 eV, reflecting an 11% increase in the power loss over that which would be calculated using a deformation potential of 15.8 eV, as deduced from the higher temperature data. We do not consider the data at this temperature to be as reliable as the higher temperature data for a number of reasons. This is the minimum temperature accessible to our system, and variations of the heat leaks into the system cause the temperature to drift. This temperature is also below the λ point of ^{4}He (the point where the He becomes a superfluid). Superfluid He is difficult to work with because of its tendency to creep along container walls. Because of this the temperature of the carbon–glass probe may not accurately reflect the lattice temperature.

The theory that is fit to the data includes the power loss to both deformation potential scattering and the power loss to piezoelectric scattering. Piezoelectric scattering

has a different temperature dependence than does deformation potential scattering, and its relative contribution to the total power loss depends on the temperature and the value of the deformation potential constant. Piezoelectric scattering dominates at low temperatures, and deformation potential scattering dominates at higher temperatures. The total contribution of piezoelectric scattering to the power loss in our experiment ranged from a maximum of approximately 20% at a lattice temperature of 1.57 K to 5% at a lattice temperature of 5.5 K, assuming a deformation potential constant of 15.8 eV. It is necessary to accurately account for the power loss to piezoelectric scattering in order to determine the value of the deformation potential constant.

In our calculation of the power loss to piezoelectric scattering we have used the generally accepted value of the piezoelectric constant, which we did not treat as an adjustable parameter. The value of the deformation potential constant necessary to fit our data did not depend on the amount of the relative contribution of piezoelectric scattering to the total power loss, despite the variation in the contribution from piezoelectric scattering, which indicates that our theory properly describes the ratio of the power losses due to each mechanism. This is in disagreement with a previously reported measurement of the power loss below 1 K which has been interpreted as indicating that the power loss to piezoelectric scattering is more than two orders of magnitude larger than expected based on theory.[59] Our experiment cannot be interpreted as showing such an anomalous power loss even if we attribute the entire measured power loss to piezoelectric scattering, and we conclude that we have seen no evidence of an anomalously large power loss to piezoelectric scattering. We note also that our experimental data cannot be explained by assuming a deformation potential constant of 7 eV and adjusting the value

of the piezoelectric constant. This model requires a 50% variation in the piezoelectric constant with lattice temperature, and it does not accurately model the temperature dependence of the experimental data at any lattice temperature.

Figure 5.2 shows the data taken at a lattice temperature of 4.2 K along with the theoretical power losses for deformation potential constants of 14.8, 15.8, and 16.8 eV. It is clear that our data is quite sensitive to the value of the deformation potential constant used, and that our results cannot be fit with deformation potential constants significantly different from 15.8 eV. Note also that a significant change in the deformation potential constant would change the percentage of the total power loss which arose from piezoelectric scattering.

We have also analyzed our data using a theory of the power loss which included a variational wave function instead of the self–consistent one. The use of the variational wave function reduces the total power loss by approximately 30% and requires a corresponding increase in the value of Z^2. This is in agreement with the findings of previous studies of scattering in heterojunctions,[28,31] and it illustrates the errors that can arise if the wave function used in the calculations does not match that of the sample.

As discussed in Chap. 3, it was not possible to distinguish experimentally between the screened and unscreened theories at the temperatures available to us. The inclusion of screening lowers the power loss at a given electron temperature, but at the temperatures of our experiment it does not change the shape of the $<d\epsilon/dt>$ versus T_e curve, and hence our data may be fit by either theory. At the electron densities available in $Al_xGa_{1-x}As$/GaAs heterostrucutures it will be necessary to make measurements below 1 K to directly observe the effects of screening, and this will require a helium dilution

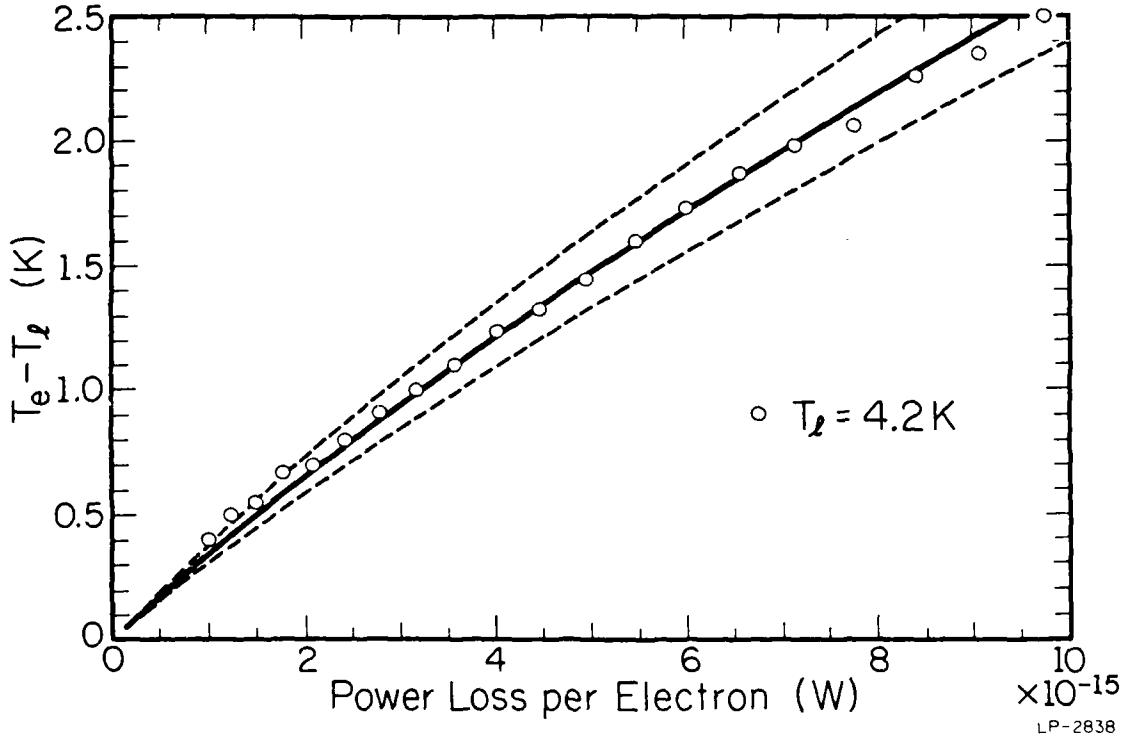

Fig. 5.2 The data at a lattice temperature of 4.2 K and the theoretical power loss calculated for deformation potentials constants of 14.8 eV, 15.8 eV, and 16.8 eV. Note that only a slight change in the deformation potential constant completely destroys the agreement between the theory and the data.

refrigerator. We find that a deformation potential constant of 11.3 eV provides the best agreement between the experimental data and the theory which does not include screening. However, in the absence of experimental data to the contrary, we believe that the theory of screening presented in Chap. 3 is a more accurate approximation than a totally unscreened theory.

5.2. Comparison with Previous Measurements in Bulk GaAs

The deformation potential constant necessary to fit our data represents a four-fold increase in acoustic phonon scattering as compared with the scattering which results if the deformation potential constant is taken to be 7 or 8 eV. As discussed in Chap. 2, we believe that the extensive studies of high–purity GaAs have convincingly established an upper limit of 11 eV for the deformation potential constant of bulk GaAs, considerably less than what we have measured in the $Al_xGa_{1-x}As$/GaAs heterojunction. This suggests that the model of scattering in heterojunctions must be drastically changed.

The model we discussed in Chap. 3 allowed for power loss through acoustic phonon scattering only. There may exist a scattering mechanism which is observed in heterojunctions, but which has not been observed in bulk material. Our measurement of the power loss, unlike measurements of the temperature dependence of the mobility, indicates clearly that such a mechanism, if it exists, is an inelastic scattering mechanism. This is an important clue to possible mechanisms. It eliminates such possibilities as interface roughness scattering, which is elastic.

A second clue comes from our ability to accurately model the power loss using an increased deformation potential constant. This indicates that any additional power loss mechanism must have a similar temperature dependence to that of deformation potential

scattering. The temperature dependence of the scattering mechanism comes from the Q dependence of the scattering matrix element. If the matrix element for a scattering mechanism has a different Q dependence, then it will not be able to explain our data. This is why, for example, we could not explain our data by fixing the deformation potential at 7 eV and adjusting the piezoelectric constant.

Recent publications[68,69] by Das Sarma et al. have suggested a possible scattering mechanism. Das Sarma has calculated the polar optic phonon spectrum including the effects of the interaction between quasiparticle excitations and the longitudinal optical phonon. This interaction produces low energy phonon modes with small spectral weight. At high temperatures these modes are dominated by the well-known 36 meV phonon mode, and their effects cannot be measured experimentally. At lower temperatures the 36 meV phonon mode is not excited in significant numbers, and the low energy phonon modes become important. Das Sarma has used this theory to resolve an important controversy regarding the power loss of electrons in heterojunctions at temperatures above approximately 30 K.

An extension of this theory to the temperatures of our experiment may explain the anomalously large power loss we observe. This mechanism has not been observed previously in measurements of the mobility in bulk GaAs because it is dominated by impurity scattering at low temperatures. It would become evident in power loss measurements, which are not affected by impurity scattering, but to our knowledge there have been no measurements of the power loss at low temperatures in bulk GaAs. It is not possible to measure the power loss in bulk GaAs using the method described in this dissertation

because of the low mobility of electron in highly doped GaAs as low temperatures. This low mobility prevents the observation of the SdH oscillations.

The anomalously large power loss may also be explained qualitatively if we assume that inhomogeneities in the $Al_xGa_{1-x}As$ – GaAs interface produce variations in the confining potential which channel current along narrow paths between the source and drain contacts. This could adversely affect our calculation of the total number of electrons in the sample, and hence our calculation of the power loss per electron. It would also change the wave function of the electron and introduce a second overlap integral which would change the magnitude of the scattering matrix element, but not its Q dependence. This explanation is therefore consistent with the observation that the temperature dependence of any additional scattering mechanism must be the same as that of deformation potential scattering. At higher temperatures this confinement potential would be small compared to the thermal energy of the electrons, and the effects would disappear. We note, however, that our observation of the SdH oscillations indicates that the electron have enough freedom to describe Landau orbits with diameters of approximately 1 μm, and that this sets a lower limit on the width of any possible channels.

Finally, as discussed in Chap. 3, a calculation of the scattering by acoustic phonons is dependent on our assumptions regarding the phonon modes. A precise calculation of the power loss may require consideration of the interface modes which result from either the $Al_xGa_{1-x}As$ – GaAs interface or from the close proximity of the crystal surface. Further experimental work to determine the importance of interface modes is necessary.

5.3. Comparison with Previous Measurements in Heterojunctions

The value of the deformation potential constant necessary to fit our data is somewhat larger than that found in most other studies of scattering in modulation doped $Al_xGa_{1-x}As/GaAs$ heterostructures. Previously reported measurements have ranged from 11 eV to 14 eV. The larger values have been reported when the data was analyzed using a variational wave function to calculate the mobility. As we have seen, the variational wave function decreases the calculated scattering rate and hence requires a larger deformation potential constant explain the data. Mendez has reanalyzed[28] data previously reported by Mendez et al.[27] He found that the deformation potential constant necessary to fit the data was reduced from 13½ eV to 12 eV when a self–consistent wave function was used in place of the variational wave function. A similar reanalysis of the other studies of the temperature dependence of the mobility would likely reduce the deformation potential constant necessary to fit the data to the 11 to 12 eV range also.

In addition to the studies of the mobility there is one recently reported study which is directly comparable to ours. Hirakawa et al. have measured the deformation potential constant through the power loss,[33] as we did, and they used a self–consistent wave function, as we did. They found that a deformation potential constant of 11 eV was necessary to fit their data. The power loss that they measured for a given electron temperature was one half of what we found. This is significantly different from our results, despite the similar structures and electron densities.

There are a number of differences between our study and previously reported studies, and these differences offer important clues as to possible causes for the differences in the measured deformation potential constant.

One important difference between our experiment and previously reported experiments is the temperature range of the data which was analyzed. The studies of the temperature dependence of the mobility cover the temperature range from approximately 5 K to 40 K. The study by Hirakawa et al. of the power loss covered a temperature range from 4.2 K to 16 K, while our study covered the temperature range from 1.6 K to 8.0 K. The temperature range of our data is wider than that of Hirakawa et al. (where the range is measured as T_{max}/T_{min}) and the absolute temperatures are lower. The data of Hirakawa et al. appears to show a larger power loss at low temperatures than can be explained using their deformation potential constant of 11 eV, which is consistent with our experimental data. We could not extend our measurements to the higher temperatures of the study by Hirakawa et al. because we used samples with lower mobilities. As discussed in Chap. 3, the Landau level broadening exponentially damps the SdH oscillations. Hence, although our low mobility samples offer the distinct advantage of Landau level broadening which is independent of T_l, they limit the maximum temperature at which we can observe the SdH oscillations. The apparent increase in the power loss which Hirakawa et al. observed at low temperatures and the large power loss which we observe may indicate that there is an additional scattering mechanism which contributes to the power loss, and that it is more effective at the low temperatures of our experiment.

A second major difference is the mobility of the samples used in these experiments. Ours is the only study of samples with mobilities less than 100 000 $cm^2\ V^{-1}\ s^{-1}$. There is no direct mechanism whereby the mobility can affect our measurements since the mobility reduction is caused by increased impurity scattering, which is elastic, and our measurements depend on the power lost through inelastic scattering mechanisms. However,

impurities might affect the power loss in some subtle way, for example, through a trapping/detrapping mechanism. Such a mechanism would be expected to have a larger effect in a low mobility sample.

The final major difference between our study and previously reported studies is the technology used to grow the crystals. The samples we have used in our study were grown by MOCVD, while all previously reported measurements have been made on samples grown by MBE. Most of the of the mechanisms which might lead to the apparent enhancement of the power loss, such as current channeling or power loss through a trapping/detrapping mechanism, would be expected to depend strongly on the growth technology. Further experimental work is necessary to determine which of the possible mechanisms is causing the observed anomalous power loss.

6. SUMMARY

We have investigated acoustic deformation potential scattering in $Al_xGa_{1-x}As/GaAs$ modulation doped heterojunctions. Because the wave function of the electron is confined almost entirely to the GaAs we expect the measured deformation potential constant to be that of bulk GaAs. However, the deformation potential constant of 11 to 14 eV which has been inferred from previous measurements of the mobility in these heterojunctions is considerably larger than the generally accepted value of 7 eV for bulk GaAs. The larger values are suspect because the maximum mobilities observed in bulk GaAs at 77 K set an upper limit of 11 eV on the deformation potential constant in bulk GaAs. Measurements based on the mobility are affected by all scattering mechanisms, which complicates the analysis of the data. We choose to investigate the power loss, which is affected only by inelastic scattering mechanisms.

We presented a theory of the electronic power loss in the heterojunction. The power loss must be computed numerically under most conditions; however, at low temperatures it may be computed analytically. When the analytical calculation is accurate, then the Q dependence of the scattering matrix element directly determines the temperature dependence of the power loss (or the mobility). Screening introduces a factor of Q^2 into the matrix element, which suggests that the theory of screening can be directly tested through its effect on the temperature dependence of the power loss. It was found that the analytical calculation of the power loss is valid only at temperatures much lower than previously believed because of the failure of equipartition.

We have measured the relationship between the electron temperature and the power loss experimentally, and we compared our experimental measurements with the theory.

In general agreement with previous measurements in heterojunctions, we found that a large value of the deformation potential constant (for our samples, approximately 16 eV) would be necessary to fit the data using the theory. In contrast with previously reported studies of acoustic deformation potential scattering in heterojunctions, we do not conclude that this indicates an error in previous measurements of Z in bulk GaAs. We suggest two possible alternatives. There may exist an additional power loss mechanism, perhaps through the low energy polar optic phonon modes which Das Sarma has described or perhaps through an impurity trapping/detrapping mechanism. Our experiment, unlike previous studies of the mobility, indicates clearly that if an additional scattering mechanism is the cause, then it must be an inelastic mechanism. Alternatively, a more sophisticated theory of scattering at low temperatures in heterojunctions, perhaps including the effects of the interface on the phonon modes, may be necessary.

APPENDIX 1. THE POWER LOSS EQUATION

In this appendix we describe in detail the steps taken in deriving the power loss equation (Eq. (3.17)) and the steps necessary for an analytic solution of it.

1.1. Derivation of the Power Loss Equation

We start from Eq. (3.16), which gives the average power loss per electron in terms of the time rate of change of the phonon mode occupation numbers,

$$<\frac{\partial\epsilon}{\partial t}> = \frac{1}{n}\sum_{Q,q}\hbar\omega_Q\frac{\partial N_Q}{\partial t}. \tag{A1.1}$$

We convert the summation over the phonon wave vector into an integral,

$$\sum_{Q,q} = (\frac{1}{2\pi})^3\int_0^\infty dQ_3\int_0^{2\pi} d\theta\int_0^{\pi} d\phi\, Q_3^2\sin\phi = (\frac{1}{2\pi})^2\int_0^\infty dQ_3\, 2\int_0^{\pi/2} d\phi\, Q_3\, Q. \tag{A1.2}$$

The $\theta = 0$ direction is arbitrary, and we integrate over θ immediately. The coordinate system is defined such that Q, the component of the phonon wave vector parallel to the heterointerface, is given by $Q = Q_3\sin\phi$, and q, the component of the phonon wave vector perpendicular to the heterointerface, is given by $q = Q_3\cos\phi$. Throughout the derivation we use Q and q freely with the understanding that these definitions are implied. To proceed further we need the expression for the time rate of change of the phonon occupation numbers, Eq. (3.12), which we reproduce here:

$$\frac{\partial N_Q}{\partial t} = 2\frac{2\pi}{\hbar}\sum_k S^2(Q)\, I^2(q)\, M^2(Q)\,\delta(\epsilon_k+\hbar\omega_Q-\epsilon_{k+Q}) \times\left\{(N_Q+1)f(\epsilon_{k+Q})[1-f(\epsilon_k)] - N_Q f(\epsilon_k)[1-f(\epsilon_{k+Q})]\right\}. \tag{A1.3}$$

We convert the summation over the two-dimensional electron wave vector into an integral over electron energy,

$$\sum_{\mathbf{k}} = (\frac{1}{2\pi})^2 \int d^2\mathbf{k} = (\frac{1}{2\pi})^2 \int_{-\pi}^{\pi} d\theta \int_0^{\infty} k\,dk = (\frac{1}{2\pi})^2 \frac{2m}{\hbar^2} \int_0^{\pi} d\theta \int_0^{\infty} d\epsilon_k, \tag{A1.4}$$

where $\theta = 0$ is defined so that θ is the angle between $\mathbf{Q}$ and $\mathbf{k}$, the components of the phonon and electron wave vectors parallel to the heterointerface. We rewrite the second line of Eq. (A1.3) as

$$\left[\exp(\hbar\omega/kT_l)\exp(-\hbar\omega/kT_e) - 1\right] N_Q f(\epsilon_k)[1-f(\epsilon_{k+Q})], \tag{A1.5}$$

where the transformation depends on our use of a Planck function characterized by the lattice temperature T_l for N_Q and a Fermi-Dirac function characterized by an elevated electron temperature T_e for $f(\epsilon)$. We also rewrite the delta function for energy conservation,

$$\delta(\epsilon_k + \hbar\omega_Q - \epsilon_{k+Q}) = \delta(\hbar\omega - \epsilon_Q - 2\cos\theta\sqrt{\epsilon_k \epsilon_Q}), \tag{A1.6}$$

where we always take the positive square root. Combining Eqs. (A1.1) through (A1.6), we find

$$\begin{aligned} <\frac{\partial \epsilon}{\partial t}> = \frac{-4m^*}{\hbar^3 (2\pi)^3} \int_0^{\infty} dQ_3\, Q_3 \left[\exp(\hbar\omega/kT_l)\exp(-\hbar\omega/kT_e) - 1\right] N_Q \\ \times \int_0^{\pi/2} d\phi\, Q\, S^2(Q)\, I^2(q)\, M^2(Q_3) \\ \times \int_0^{\infty} d\epsilon_k \int_0^{\pi} d\theta\, f(\epsilon_k)[1 - f(\epsilon_{k+Q})]\, \delta(\hbar\omega - \epsilon_Q - 2\cos\theta\sqrt{\epsilon_k \epsilon_Q}). \end{aligned} \tag{A1.7}$$

We now define

$$\Delta E \equiv \epsilon_Q + 2\cos\theta\sqrt{\epsilon_k \epsilon_Q}, \tag{A1.8}$$

and

$$d(\Delta E) = -2\sqrt{\epsilon_k \epsilon_Q}\left[1 - \frac{(\Delta E - \epsilon_Q)^2}{4\epsilon_k \epsilon_Q}\right]^{1/2} d\theta. \tag{A1.9}$$

We convert the integral over θ to one over ΔE to get

$$<\frac{\partial\epsilon}{\partial t}> = \frac{2m^*}{\hbar^3(2\pi)^3}\int_0^\infty dQ_3\, Q_3 \left[\exp(\hbar\omega/kT_l)\exp(-\hbar\omega/kT_e) - 1\right] N_Q$$
$$\times \int_0^{\pi/2} d\phi\, Q\, S^2(Q)\, I^2(q)\, M^2(Q_3) \int_0^\infty d\epsilon_k \qquad \text{(A1.10)}$$
$$\times \int_{\Delta E_{min}}^{\Delta E_{max}} d(\Delta E)(\epsilon_k\epsilon_Q)^{-1/4} \left[1 - \frac{(\Delta E - \epsilon_Q)^2}{4\epsilon_k\epsilon_Q}\right]^{-1/2} f(\epsilon_k)[1 - f(\epsilon_{k+Q})]\delta(\hbar\omega - \Delta E),$$

where

$$\Delta E_{min} = \epsilon_Q - 2\sqrt{\epsilon_k\epsilon_Q}, \qquad \text{(A1.11)}$$

and

$$\Delta E_{max} = \epsilon_Q + 2\sqrt{\epsilon_k\epsilon_Q}. \qquad \text{(A1.12)}$$

We evaluate the integral over ΔE using the properties of the delta function. The requirement that $\hbar\omega$ lie within the range between ΔE_{min} and ΔE_{max} is satisfied if the electron has a minimum energy. The power loss is then

$$<\frac{\partial\epsilon}{\partial t}> = \frac{2u\sqrt{2m^*}}{\hbar\epsilon_f(2\pi)^2}\int_0^\infty dQ_3\, Q_3^2 \left[\exp(\hbar\omega/kT_l)\exp(-\hbar\omega/kT_e) - 1\right] N_Q$$
$$\times \int_0^{\pi/2} d\theta\, S^2(Q)\, I^2(q)\, M^2(Q_3) \qquad \text{(A1.13)}$$
$$\times \int_{\epsilon_{min}}^\infty d\epsilon_k\, \epsilon_k^{-1/4} \left[1 - \frac{(\hbar\omega - \epsilon_Q)^2}{4\epsilon_k\epsilon_Q}\right]^{-1/2} f(\epsilon_k)[1 - f(\epsilon_k + \hbar\omega)],$$

where the minimum electron energy is

$$\epsilon_{min} = \frac{(\hbar\omega - \epsilon_Q)^2}{4\epsilon_Q}, \qquad \text{(A1.14)}$$

and where we have used the two-dimensional density of states to relate n to ϵ_f. Further simplification of the power loss equation requires a number of approximations, which we discuss in the next section.

1.2. The Approximate Analytical Solution

With certain approximations, it is possible to solve for the average power loss analytically. Our starting point is Eq. (3.17), derived in App. 1.1, To solve this equation analytically, we must make some approximations. As discussed in Chap. 3, the main approximations are the replacement of the overlap integral I(q) by unity, the use of the strong screening approximation, $S(Q) = Q/P$, and the approximation $N_Q = \exp(-\hbar\omega/kT)$ for the phonon occupation numbers. With these approximations we can reduce Eq. (A1.14) to

$$<\frac{\partial\epsilon}{\partial t}> = F(T_e) - F(T_l), \tag{A2.1}$$

where

$$F(T) = \frac{2u\sqrt{2m^*}}{\hbar\epsilon_f(2\pi)^2}\int_0^\infty dQ_3 Q_3^2 \exp(-\hbar\omega/kT)\int_0^{\pi/2} d\theta \frac{Q^2}{P^2}M^2(Q_3) \times \int_{\epsilon_{min}}^\infty d\epsilon_k(\epsilon_k)^{-1/4} f(\epsilon_k)[1 - f(\epsilon_k + \hbar\omega)]\left[1 - \frac{(\hbar\omega - \epsilon_Q)^2}{4\epsilon_k\epsilon_Q}\right]^{-1/2}. \tag{A2.2}$$

Some other minor approximations are necessary to the solution of this equation. The integral over ϵ_k contains a factor

$$\left[1 - \frac{(\hbar\omega - \epsilon_Q)^2}{4\epsilon_k\epsilon_Q}\right]^{-1/2} \cong \left[1 - \frac{Q}{4k_f}\right]^{-1/2} \cong 1, \tag{A2.3}$$

for small Q. This approximation will be accurate at any temperature for which the other approximations are accurate. This integral also contains a factor $\epsilon_k^{-1/4}$. This factor varies slowly in comparison with the rest of the integrand, and we take it to be constant at the point where the integral peaks, $\epsilon_k \cong \epsilon_f$. If we also replace the lower limit of the integral with $-\infty$, an excellent approximation for a degenerate system, then the remaining integral can be solved analytically, and has the value $\hbar\omega$. With these approximations, we

now have

$$F(T) = \frac{2u^2\sqrt{2m^*}}{(P\epsilon_f 2\pi)^2}\int_0^\infty dQ_3\, Q_3^5 \exp(-\hbar\omega/kT)\int_0^{\pi/2} d\phi \sin^2\phi M^2(Q_3). \tag{A2.4}$$

To proceed further we must choose a specific matrix element M(Q). The matrix element for deformation potential scattering is

$$M^2(Q_3) = \frac{Z^2\hbar Q_3}{2\rho u_l}. \tag{A2.5}$$

We substitute into Eq. (A2.4) and integrate over θ, and substitute from Eq. (3.10) for the constant P, to get

$$F(T) = \frac{u_l\epsilon^2 Z^2\hbar^5}{\epsilon_f^2(2\pi)^2(2m^*)^{3/2}e^4\rho}\int_0^\infty dQ_3\, Q_3^6 \exp(-\hbar\omega/kT). \tag{A2.6}$$

Finally, we define

$$x \equiv \frac{\hbar u Q_3}{kT}, \tag{A2.7}$$

and

$$dx = \frac{\hbar u}{kT} dQ_3. \tag{A2.8}$$

With this substitution we find

$$F(T) = \frac{6!\epsilon^2 Z^2 (kT)^7}{\epsilon_f^2(2\pi)^2(2m^*)^{3/2}e^4\rho\hbar^2 u_l^6}, \tag{A2.9}$$

which concludes our derivation of the analytical equation for the power loss to screened deformation potential scattering. The analytical solution for the power loss to piezoelectric scattering may be obtained similarly.

REFERENCES

1 W. Shockley, U. S. Patent 2,569,347 (1951).

2 For a review, see L. M. Miller and J. J. Coleman, "A Critical Review of Metal Organic Chemical Vapor Deposition," CRC Critical Reviews, in press.

3 For a review, see W. T. Tsang, "MBE for III-V Compound Semiconductors," in *Semiconductors and Semimetals*, edited by R. K. Willardson and A. C. Beer, (Academic Press, New York, 1985) Vol. 22, part A, 95–207.

4 For a review, see T. Mimura, K. Nishiuchi, M. Abe, A. Shibatomi, and M. Kobayashi, "Status and Trends of Hemt Technology," Superlattices and Microstructures **1**, 369–373 (1985).

5 For example, see K. Hess, H. Morkoç, H. Shichijo, and B. G. Streetman, "Negative Differential Resistance Through Real-Space Electron Transfer," Appl. Phys. Lett. **35**, 469–471 (1979); Serge Luryi, Alexander Kastalsky, Arthur C. Gossard, and Rudi H. Hendel, "Charge Injection Transistor Based on Real-Space Hot-Electron Transfer," IEEE Trans. Electron Devices, **ED–31**, 832–839, (1984).

6 For a review, see Richard E. Prange and Steven M. Girvin, editors, *The Quantum Hall Effect*, Springer–Verlag, New York, (1987).

7 B. R. Nag, *Theory of Electrical Transport in Semiconductors*, Pergamon Press, New York (1972).

8 J. David Zook, "Piezoelectric Scattering in Semiconductors," Phys. Rev. **136**, A869–A878 (1964).

9 For example, see K. G. Hambleton, "The Sign of the Effective Ionic Charge in Gallium Arsenide," Phys. Letters **16**, 241–242 (1965).

10 J. Bardeen and W. Shockley, "Deformation Potentials and Mobilities in Non–Polar Crystals," Phys. Rev. **80**, 72–80 (1950).

11 R. Dingle, H. L. Störmer, A. C. Gossard, and W. Wiegmann, "Electron Mobilities in Modulation–Doped Semiconductor Heterojunction Superlattices," Appl. Phys. Lett., **33**, 665–667 (1978).

12 For further discussion of deformation potential scattering at heterointerfaces, see K. K. Mon, K. Hess, and J. D. Dow, "Deformation Potentials of Superlattices and Interfaces," J. Vac. Sci. Technol. **19**, 564–566 (1981).

13 C. M. Wolfe, G. E. Stillman, and W. T. Lindley, "Electron Mobility in High–Purity GaAs," J. Appl. Phys. **41**, 3088–3091 (1970).

14 H. J. Lee, J. Basinski, L. Y. Juravel, and J. C. Woolley "Electrical Transport and Band Structure of GaAs," Can. J. Phys. **57**, 233–242 (1979).

15 D. L. Rode and S. Knight "Electron Transport in GaAs," Phys. Rev. B **40**, 2534–2541 (1969).

16 S. Perkowitz, "Mobility and Infrared Absorption in *n*–type Gallium Arsenide," J. Appl. Phys. **40**, 3651–3754 (1969).

17 Eijiro Haga and Hatsuo Kimura, "Free–Carrier Absorption in III–V Semiconductors III. GaAs, InP, GaP, and GaSb," J. Phys. Soc. Japan **19**, 658–669 (1964).

18 J. S. Harris, Ph. D. dissertation, Stanford University, 1968, unpublished. Referenced in L. W. James and J. L. Moll, "Transport Properties of GaAs Obtained from Photoemission Measurements," Phys. Rev. **183**, 740–753 (1969).

19 H. Ehrenreich, "Band Structure and Electron Transport of GaAs," Phys. Rev. **120**, 1951–1963 (1960).

20 D D. Notte, W. Walukiewicz, and E. E. Haller, "Band Edge Hydrostatic Deformation Potentials in III–V Semiconductors," Phys. Rev. Lett. **59**, 501–504 (1987).

21 Pawel Pfeffer and Iza Gorczyca "Theory of Free–Electron Absorption in *n*–GaAs," Solid State Commun. **51**, 179–183 (1984).

22 D. C. Look and P. C. Colter, "Electrical Properties of Low–Compensation GaAs," Phys. Rev. B **28**, 1151–1153 (1983).

23 W. Walukiewicz, H. E. Ruda, J. Lagowski, and H. C. Gatos, "Response to 'Comment on 'Electron Mobility in Modulation–Doped heterostructures'," Phys. Rev. B **32**, 2645–2646 (1985). See also Reference 29.

24 D. L. Rode, "Low–Field Electron Transport," in *Semiconductors and Semimetals*, edited by R. K. Willardson and A. C. Beer, (Academic Press, New York, 1975) Vol. 10, 1–89.

25 Code written in Fortran by Matt Kim, University of Illinois.

26 G. E. Stillman and C. M. Wolfe, "Electrical Characterization of Epitaxial Layers," Thin Solid Films **31**, 69–88 (1976).

27 E. E. Mendez, P. J. Price, and M. Heiblum, "Temperature Dependence of the Electron Mobility in GaAs-GaAlAs heterostructures," Appl. Phys. Lett. **45**, 294–296 (1984).

28 E. E. Mendez, "Electronic Mobility in Semiconductor Heterostructures," IEEE J. Quantum Electron., **QE–22**, 1720–1727 (1986).

29 Peter J. Price, "Comment on 'Electron Mobility in Modulation–Doped Heterostructures'," Phys. Rev. B **32**, 2643–2644 (1985). See also Reference 23.

30 B. J. F. Lin, D. C. Tsui, and G. Weimann, "Mobility Transition in the Two–Dimensional Electron Gas in GaAs–AlGaAs Heterostructures," Solid State Commun. **56**, 287–290 (1985).

31 B. Vinter, "Low–Temperature Phonon–Limited Electron Mobility in Modulation–Doped Heterostructures," Phys. Rev. B **33**, 5904–5905 (1986).

32 Kazuhiko Hirakawa and Hiroyuki Sakaki, "Mobility of the Two–Dimensional Electron Gas at Selectively Doped *n*–Type $Al_xGa_{1-x}As$/GaAs Heterojunctions With Controlled Electron Concentrations," Phys. Rev. B **32**, 8291–8303 (1986).

33 Kazuhiko Hirakawa and Hiroyuki Sakaki, "Energy Relaxation of Two–Dimensional Electrons and the Deformation Potential Constant in Selectively Doped AlGaAs/GaAs Heterojunctions," Appl. Phys. Lett. **49**, 889–891 (1986).

34 Peter J. Price, "Low Temperature Two-Dimensional Mobility of a GaAs Heterolayer," Surf. Sci. **143**, 145–156 (1984).

35 G. Bauer, "Determination of Electron Temperature and of Hot Electron Distribution Functions in Semiconductors," in *Springer Tracts in Modern Physics*, (Springer–Verlag, New York, 1974) Vol. 74, 1–106.

36 R. E. Peierls, *Quantum Theory of Solids*, Oxford University Press, London (1974).

37 For a review, see M. V. Kline, "Phonons in Semiconductor Superlattices," IEEE J. Quantum Electron. **QE–22**, 1760–1770 (1986).

38 Hiroshi Ezawa, Shinji Kawaji, and Koichi Nakamura, "Surfons and the Electron Mobility in Silicon Inversion Layers," Japan J. Appl. Phys. **13**, 126–155 (1974).

39 Hiroshi Ezawa, Shinji Kawaji, and Koichi Nakamura, "Surfons and the Electron Mobility in a Semiconductor Inversion Layer," Surf. Sci. **27**, 218–220 (1971).

40 Hiroshi Ezawa, Toshio Kuroda, and Koichi Nakamura, "Electrons and 'Surfons' in a Semiconductor Inversion Layer," Surf. Sci. **24**, 654–658 (1971).

41 K. Hess, "Aspects of High–Field Transport in Semiconductor Heterolayers and Semiconductor Devices," in *Advances in Electronics and Electron Physics*, edited by P. W. Hawkes, (Academic Press, New York 1982) Vol. 59, 239–306.

42 D. K. Ferry, "Fundamental Aspects of Hot Electron Phenomena," in *Handbook on Semiconductors*, edited by T. S. Moss, (North–Holland Publishing Company, 1982) Vol. 1, 563–597.

43 E. Vass, "Study of the Energy Relaxation time of Hot Electrons in GaAs/GaAlAs Heterostructures," Physica 134B&C, 337–341 (1985).

44 N. W. Ashcroft and N. D. Mermin, *Solid State Physics*, Holt, Rinehart and Winston, New York (1976).

45 J. Batey and S. L. Wright, "Energy Band Alignment in GaAs/(Al,Ga)As Heterostructures: the Dependence on Alloy Composition," J. Appl. Phys. **59**, 200–209 (1986).

46 R. Dingle, W. Wiegmann, and C. H. Henry, "Quantum States of Confined Carriers in Very Thin $Al_xGa_{1-x}As$ – GaAs – $Al_xGa_{1-x}As$ Heterostructures," Phys. Rev. Lett. **33**, 827–830 (1974).

47 T. W. Hickmott, P. M. Solomon, R. Fischer, and H. Morkoç, "Negative Charge, Barrier Heights, and the Conduction–Band Discontinuity in $Al_xGa_{1-x}As$ Capacitors," J. Appl. Phys. **57**, 2844–2853 (1985).

48 R. C. Miller, A. C. Gossard, D. A. Kleinman, and O. Munteanu, "Parabolic Quantum Wells with the GaAs – $Al_xGa_{1-x}As$ System," Phys. Rev. B **29**, 3740–3744 (1984);

49 R. C. Miller, D. A. Kleinman, and A. C. Gossard, "Energy–Gap Discontinuities and Effective Masses for GaAs – $Al_xGa_{1-x}As$ Quantum Wells," Phys. Rev. B **29**, 7085–7087 (1984).

50 T. Ando, A. B. Fowler, and F. Stern, "Electronic Properties of Two–Dimensional Systems," Rev. Mod. Phys. **54**, 437–672 (1982).

51 K. Yokoyama and K. Hess, "Intersubband Phonon Overlap Integrals for AlGaAs/GaAs Single–Well Heterostructures," Phys. Rev. B **31**, 6872–6874 (1986).

52 W. Walukiewicz, H. E. Ruda, J. Lagowski, and H. C. Gatos, "Electron Mobilities in Modulation–Doped Heterostructures," Phys. Rev. B **30**, 4571–4582 (1984).

53 P. J. Price, "Two–Dimensional Electron Transport in Semiconductor Layers II: Screening," J. Vac. Sci. Technol. **19**, 599–603 (1981).

54 K. Hess, *Advanced Theory of Semiconductor Devices*, Prentice Hall, Englewood Cliffs, (1988).

55 E. M. Conwell, "High Field Transport in Semiconductors," in *Solid State Physics*, edited by F. Seitz, D. Turnbull, and H. Ehrenreich, (Academic Press, New York, 1967) supplement, Vol. 9, 1-293.

56 P. J. Price, "Two–Dimensional Electron Transport in Semiconductor Layers I: Phonon Scattering," Ann. Phys. (N.Y.) **133**, 217–239 (1981).

57 K. Hess, T. Englert, T. Neugebauer, G. Landwehr, and G. Dorda, "Hot–Carrier Effect in High Magnetic Fields in Silicon Inversion Layers at Low Temperatures: *p* Channel," Phys. Rev. B. **16**, 3652–3659 (1977); for experimental applications, see T. Neugebauer and G. Landwehr, "Determination of the Phonon Modes Involved in the Carrier–Phonon Interaction in Silicon Inversion Layers at Low Temperatures by Nonohmic Transport Measurements," Phys. Rev. B. **21**, 702–708 (1980).

58 P. J. Price, "Hot Electrons in a GaAs Heterolayer at Low Temperature," J. Appl. Phys. **53**, 6863–6866 (1982).

59 S. J. Manion and K. Hess, "Phonon Energy Dependence of Scattering in Quasi–Two–Dimensional Electron Gases at Low Temperature," J. Appl. Phys. **62**, 4942–4944 (1987).

60 A. K. M. Wennberg, S. N. Ytterboe, C. M. Gould, H. M. Bozler, J. Klem, and H. Morkoç, "Electron Heating in a Multiple Quantum–Well Structure Below 1 K," Phys. Rev. B **34**, 4409–4411 (1986).

61 Janos Hajdu and Gottfried Landwehr, "Quantum Transport Phenomena in Semiconductors in High Magnetic Fields," in *Topics in Applied Physics: Strong and Ultrastrong Magnetic Fields*, edited by F. Herlach (Springer–Verlag, New York, 1985) Vol. 57, 17–112.

62 L. D. Landau and E. M. Lifshitz *Quantum Mechanics*, 3rd edition, Pergamon Press, New York (1977).

63 H. Weiss, "Magnetoresistance," in *Semiconductors and Semimetals*, (Academic Press, New York, 1966) Vol. 1, 315–374.

64 B. L. Altshuler, D. K.hmelnitzkii, A. I. Larkin, and P. A. Lee, "Magnetoresistance and Hall Effect in a Disordered Two-Dimensional Electron Gas," Phys. Rev. B **22**, 5142–5153 (1980).

65 P. A. Lee and T. V. Ramakrishnan, "Magnetoresistance of Weakly Disordered Electrons," Phys. Rev. B **26**, 4009-4012 (1988).

66 E. F. Schubert, K. Ploog, H. Dämbkes, and K. Heime, "Selectively Doped n–$Al_xGa_{1-x}As$/GaAs Heterostructures with High–Mobility Two–Dimensional Electron Gases for Field Effect Transistors. Part I. Effect of Parallel Conductance," Appl. Phys. A. **33**, 63–76 (1984).

67 S. J. Manion, M. Artaki, M. A. Emanuel, J. J. Coleman, and K. Hess, "Electron–Energy–Loss Rates in $Al_xGa_{1-x}As$/GaAs Heterostructures at Low Temperatures," Phys. Rev. B **35**, 9203–9208 (1987).

68 S. Das Sarma, J. K. Jain, and R. Jalabert, "Hot–Electron Relaxation in GaAs Quantum Wells," Phys. Rev. B **37**, 1228–1230 (1988).

69 S. Das Sarma, J. K. Jain, and R. Jalabert, "Effect of Phonon Self–Energy Correction on Hot–Electron Relaxation in Two–Dimensional Semiconductor Systems," Phys. Rev. B **37**, 4560–4566 (1988).

VITA

Stephen Joseph Manion [redacted] graduated from Pocomoke High School in 1977. He continued his education at the University of Delaware and in 1981 was graduated with a Bachelor of Electrical Engineering degree. From 1981 to 1988 he studied electrical engineering under the guidance of Professor Karl Hess at the University of Illinois at Urbana–Champaign. He received his Master of Science degree in 1985. Mr. Manion is currently a candidate for the degree of Doctor of Philosophy degree.

Mr. Manion is a member of Tau Beta Pi, Eta Kappa Nu, The Institute of Electrical and Electronics Engineers, The American Physical Society, and the American Association for the Advancement of Science.

END

DATE

FILMED

DTIC

10-88